Journal of Sound and Vibration 540 (2022) 117247

Contents lists available at ScienceDirect

Journal of Sound and Vibration

journal homepage: www.elsevier.com/locate/jsvi

Nonlinear Modes in Shear Horizontal Wave Propagation–Analytical and Numerical Analysis

M. Osika [a], A. Ziaja-Sujdak [a], R. Radecki [a], L. Cheng [b], W.J. Staszewski [a,*]

[a] Department of Robotics and Mechatronics, AGH University of Science and Technology, Al. A. Mickiewicza 30, Krakow, 30-059, Poland
[b] Department of Mechanical Engineering, The Hong Kong Polytechnic University, Kowloon, Hong Kong, China

ARTICLE INFO

Keywords:
Shear horizontal waves
Material nonlinearity
Nonlinear wave propagation
Nonlinear modes
Distorted dispersion curves

ABSTRACT

Nonlinear shear horizontal guided wavefield is investigated analytically in plates. The major focus is on the effect of nonlinear material parameters, excitation frequency, wave number and wave amplitude on nonlinear mode generation. The analytical solution is based on the multiple-scale perturbation method and modal decomposition approach. The approximate analytical solution is validated using the Local Interaction Simulation Approach, implemented for nonlinear shear wave propagation. The results show that the analysed shear horizontal wavefield is distorted by material nonlinearity. The resulting displacement field can be interpreted in a form of nonlinear modes.

1. Introduction

Most engineering structures require monitoring for material defects, material degradation and structural damage to maintain safe operation and to minimise costs of ownership. Therefore manufacture and maintenance of such structures require reliable methods for material evaluation and early detection of structural defects. Methods that utilise ultrasonic waves are attractive for this task. Various approaches based on wave propagation phenomena – such as attenuation, reflection or scattering – have been proposed and implemented for field testing [1]. Classical, non-destructive ultrasonic testing, that relies on well-established actuation/sensing and data processing techniques, has led to a relatively widespread range of applications for many years. Guided ultrasonic waves and their propagation have been also considered for material testing and damage detection, particularly in plate-like structures [2].

Recent years have brought more research interest in nonlinear ultrasonic methods. It is widely accepted that these methods – although more difficult for practical implementation – offer high sensitivity to early-stage defects even at a microstructural level [3–6]. In general, nonlinearities observed in measured ultrasonic responses result from four major sources: (1) material (e.g., grain structures, inclusions, elastic and attenuation properties), (2) defects (e.g. cracks in metals, delaminations in composites), (3) structural assemblies (e.g. joint friction) and (4) intrinsic effects (instrumentation chain — e.g. overloads). However, the last source cannot be considered as wave propagation nonlinearity and relates to undesired experimental errors (e.g., nonlinear coupling of transducer). Physical mechanisms of the first two sources (i.e., material and defects) are of particular interest to non-destructive testing and structural health monitoring research communities.

Nonlinear ultrasonic wave propagation and the problem of higher harmonic generation have been studied theoretically and implemented for material defect detection for decades since the early work in the 1960s [7,8]. The vast majority of these investigations relates to nonlinear bulk and surface waves [1,3–5]. More recently, nonlinear guided waves have been investigated. The effect of material nonlinearity on Lamb wave propagation has been extensively studied from theoretical [9,10], numerical [11–14] and experimental [15–17] standpoints. These research investigations have revealed the generation mechanism of higher

* Corresponding author.
E-mail address: w.j.staszewski@agh.edu.pl (W.J. Staszewski).

https://doi.org/10.1016/j.jsv.2022.117247
Received 22 February 2022; Received in revised form 27 July 2022; Accepted 13 August 2022
Available online 18 August 2022
0022-460X/

harmonics for waves propagating in hyperelastic medium, showing the great potential for early damage detection. Deng [9] theoretically described the physical process of cumulative second-harmonic generation of nonlinear Lamb wave propagation. This work has involved the straightforward expansion technique (i.e., basic perturbation analysis [18]) and the reciprocity relation [19] to define the synchronism conditions between the primary and the secondary Lamb wave modes.

The analytical approach based on the perturbation technique has been also adopted to investigate the interaction between Lamb waves and Shear Horizontal (SH) waves [20,21]. This work demonstrates that that the Lamb wave primary wavefield, cannot excite higher harmonics of SH guided waves in semi-infinite medium. In contrast, research investigations in [22,23] shows that the generation of Lamb wave secondary wavefield by primary SH waves can be observed in a nonlinear material. It is important to note that these combined Lamb and SH wave interactions have been investigated mainly with respect to excitation.

The theoretical studies on nonlinear guided wave propagation presented in the aforementioned publications — show that in approximate solutions (i.e., solutions based on the straightforward expansion perturbation technique [18]) amplitudes of higher harmonic components increase infinitely with the direction of wave propagation at synchronism points. This effect limits the validity of approximate solutions to short time and distance of wave propagation. Approximate solutions are analysed in [24,25] for nonlinear wave propagation problems and selected variants of perturbation methods. More recently, other variants of perturbation techniques, which prevent the secular terms in approximation solutions, have been proposed for investigations of nonlinear guided waves. The Lindstedt–Poincare technique has been used in [26] to investigate the effect of nonlinear material parameters and the excitation amplitude/frequency on dispersion characteristics of nonlinear Lamb waves. The multiple-scale method has been used in [27] to investigate the interaction between two Lamb modes in the presence of linear damping. Cyclic energy transfer between primary and secondary modes with the propagation distance, which is analytically predicted by introducing the detuning parameter, has been also investigated in [25]. The results with damping effects show attenuation of both amplitudes with propagation distance. This behaviour limits propagation distance of resonance Lamb wave modes.

In summary, it appears that in contrast to nonlinear Lamb waves, nonlinear SH wave propagation has not been investigated in depth. The conditions for cumulative second-harmonic generation for nonlinear SH modes have been studied in [6,28,29]. These analytical approaches have been based on the straightforward expansion perturbation technique for nonlinear elastodynamic governing equations and boundary conditions. The partial wave technique, modal decomposition and reciprocity relation [19] have been used to solve mathematical problems resulting from the application of this perturbation method. The potential of the nonlinear SH wave propagation for early detection of material degradation has been discussed in the recent tutorial [6]. However, the distortion of the primary wavefield due to material nonlinearity has not been investigated. The current paper attempts to fill this gap. The objective of the paper is the analytical study of the nonlinear SH wavefield, i.e. higher harmonics generation and nonlinear SH modes. The major novelty of the work presented relates to two elements. Firstly, the paper investigates the effect of nonlinear material parameters, excitation frequency, wave number and wave amplitude on distortion of dispersion curves for primary wavefield. Secondly, nonlinear modes in shear wave propagation – due to material nonlinearity – are observed.

The paper is organised as follows. Section 2 starts with the theoretical background. The nonlinear SH wave propagation problem is formulated. The analytical solution is presented in Section 3. The multiple-scale perturbation method and modal decomposition approach are used to obtain the approximate solution. The analytical solutions are validated using numerical simulations in Section 4. The Local Interaction Simulation Approach – developed for the nonlinear guided SH wavefield – is used to obtain the approximate numerical solution. Finally, the work is concluded in Section 5.

2. Shear horizontal waves in nonlinear medium-theory

2.1. Problem description

Elastic guided waves can only exist in bounded media. Plate-like structures are examples of systems for which they can be observed. Multiple reflections of propagating bulk waves from boundaries lead to generation of an infinite number of modes with corresponding dispersion relations. In this paper, an infinite plate bounded by two parallel stress-free surfaces is considered. Fig. 1 shows a schematic geometric model of the considered system with marked global Cartesian coordinates indicating components of displacements of individual particles. The invariance along the z-direction is assumed, so the entire analysis is reduced to the selected cross-section of the plate. In addition, the study focuses on SH waves, so mechanical constraints are imposed on the system and described herein.

The problem of linear propagation of guided waves can be considered as based on the method of eigenfunction (modal shape) expansion [30]. The general motion of the linear system can be expressed as a superposition of responses for each normal mode. The work in this paper focuses on the propagation of SH guided waves in a nonlinear elastic medium. So, superposition does not hold and the problem cannot be directly analysed using this approach. Thus, the analysis based on the approximate method is employed. This section presents the mathematical model of SH nonlinear guided wave propagation problem i.e., the governing equation with the definition of boundary conditions and the approximate solution based on the multiple-scale perturbation technique.

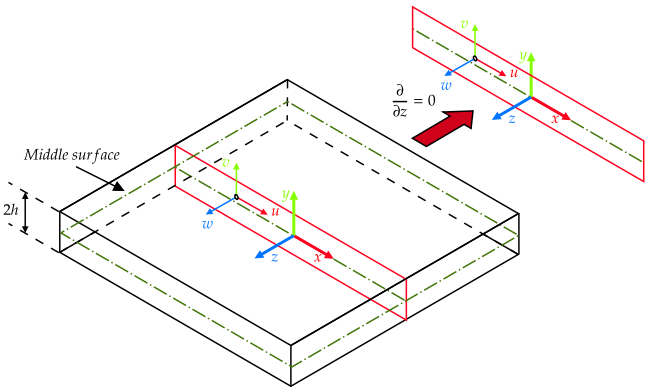

Fig. 1. Geometrical model of the considered system and used coordinates.

2.2. Waves in unbounded elastic medium

For an isotropic elastic medium, the elastodynamic stress equation of motion, namely the Navier equation is given by

$$\tilde{\mathbf{F}} + \nabla\boldsymbol{\sigma} = \rho\frac{\partial^2\mathbf{W}}{\partial t^2}, \tag{1}$$

where ρ, t, $\boldsymbol{\sigma}$, $\tilde{\mathbf{F}}$ and $\mathbf{W}$ are material density, time, stress tensor, body force vector and displacement vector, respectively. The mathematical relationship between individual components of $\boldsymbol{\sigma}$ and $\mathbf{W}$ is in general nonlinear. The analytical expression of this nonlinear relation results from the assumed geometric definition of strain and the constitutive equation between stress and strain tensors components.

In this paper, small but finite amplitude waves are considered. Therefore, the Green–Lagrange strain tensor definition is assumed as

$$\boldsymbol{\varepsilon_{GL}} = \frac{1}{2}(\mathbf{H} + \mathbf{H}^T + \mathbf{H}^T\mathbf{H}), \tag{2}$$

where $\mathbf{H}$ is the gradient of the displacement field. The second Piola–Kirchhoff stress tensor – previously used in numerical simulations [31] – is employed as a measure of stress field. Each of its components is given by [22]

$$\sigma_{ij} = \frac{\partial U(\boldsymbol{\varepsilon_{GL}})}{\partial(\varepsilon_{GL})_{ij}}, \tag{3}$$

where $U(\boldsymbol{\varepsilon_{GL}})$ is strain energy density and subscripts $i, j \in \{x, y, z\}$. The Landau–Lifshitz nonlinear model [32] is adopted to characterise properties of hyper-elastic material. The extension to the fourth order of strain energy density $U(\boldsymbol{\varepsilon_{GL}})$ is given by

$$U(\boldsymbol{\varepsilon_{GL}}) = \frac{\lambda}{2}I_1^2 + \mu I_2 + \frac{\mathcal{A}}{3}I_3 + \mathcal{B}I_1I_2 + \frac{\mathcal{C}}{3}I_1^3 + \mathcal{E}I_1I_3 + \mathcal{F}I_1^2I_2 + \mathcal{G}I_2^2 + \mathcal{H}I_1^4, \tag{4}$$

where λ, μ are the Lamé elastic constants, $\mathcal{A}$, $\mathcal{B}$, $\mathcal{C}$ are the Third Order Elastic Constants (TOEC) and $\mathcal{E}$, $\mathcal{F}$, $\mathcal{G}$, $\mathcal{H}$ are the Fourth Order Elastic Constants (FOEC) [33]. The scalars I_1, I_2 and I_3 denote the first, second and third invariants of the Green–Lagrange strain tensor $\boldsymbol{\varepsilon_{GL}}$, respectively and are defined as

$$\begin{aligned} I_1 &= \mathrm{tr}(\boldsymbol{\varepsilon_{GL}}),\\ I_2 &= \mathrm{tr}(\boldsymbol{\varepsilon_{GL}}^2),\\ I_3 &= \mathrm{tr}(\boldsymbol{\varepsilon_{GL}}^3). \end{aligned} \tag{5}$$

As mentioned in the problem description, the invariance along z axis i.e., $\frac{\partial}{\partial z} = 0$ is assumed. For a linear material, this assumption leads to the decoupling of the wave equation; one part corresponds to SH waves and the other two equations describe Lamb wave propagation. This property is not true for a nonlinear material model considered. The nonlinear terms in definition of stress components result in the coupling between these equations [22,23]. Therefore, in this work to analyse only SH waves, the following assumptions $\mathbf{W} = [0,\ 0,\ w]^T$, $\tilde{\mathbf{F}} = [0,\ 0,\ \tilde{F}_z]^T$ are made. This means that the displacements and the mass forces components corresponding to x and y directions are negligible. Consequently, the general mathematical model from Eq. (1) reduces from a vector equation to a one (scalar) partial differential equation

$$\tilde{F}_z + \frac{\partial\sigma_{xz}}{\partial x} + \frac{\partial\sigma_{yz}}{\partial y} = \rho\frac{\partial^2 w}{\partial t^2}. \tag{6}$$

The components of the second Piola–Kirchhoff stress tensor in Eq. (6) for the Landau–Lifshitz strain energy density defined by Eq. (4) can be expressed as

$$\begin{aligned} \sigma_{xz} = {} & 2\mu\varepsilon_{xz} + \mathcal{A}(\varepsilon_{xx}\varepsilon_{xz} + \varepsilon_{xy}\varepsilon_{yz} + \varepsilon_{xz}\varepsilon_{zz}) + 2\mathcal{B}\varepsilon_{xz}(\varepsilon_{xx} + \varepsilon_{yy} + \varepsilon_{zz}) + 3\mathcal{E}(\varepsilon_{xx} + \varepsilon_{yy} + \varepsilon_{zz})(\varepsilon_{xx}\varepsilon_{xz} + \varepsilon_{xy}\varepsilon_{yz} + \varepsilon_{xz}\varepsilon_{zz})\\ & + 2\mathcal{F}\varepsilon_{xz}(\varepsilon_{xx} + \varepsilon_{yy} + \varepsilon_{zz})^2 + 4\mathcal{G}\varepsilon_{xz}(\varepsilon_{xx}^2 + 2\varepsilon_{xy}^2 + 2\varepsilon_{xz}^2 + \varepsilon_{yy}^2 + 2\varepsilon_{yz}^2 + \varepsilon_{zz}^2), \end{aligned} \tag{7}$$

$$\sigma_{yz} = 2\mu\varepsilon_{yz} + \mathcal{A}(\varepsilon_{xy}\varepsilon_{xz} + \varepsilon_{yy}\varepsilon_{yz} + \varepsilon_{yz}\varepsilon_{zz}) + 2\mathcal{B}\varepsilon_{yz}(\varepsilon_{xx} + \varepsilon_{yy} + \varepsilon_{zz}) + 3\mathcal{E}(\varepsilon_{xx} + \varepsilon_{yy} + \varepsilon_{zz})(\varepsilon_{xy}\varepsilon_{xz} + \varepsilon_{yy}\varepsilon_{yz} + \varepsilon_{yz}\varepsilon_{zz}) + 2\mathcal{F}\varepsilon_{yz}(\varepsilon_{xx} + \varepsilon_{yy} + \varepsilon_{zz})^2 + 4\mathcal{G}\varepsilon_{yz}(\varepsilon_{xx}^2 + 2\varepsilon_{xy}^2 + 2\varepsilon_{xz}^2 + \varepsilon_{yy}^2 + 2\varepsilon_{yz}^2 + \varepsilon_{zz}^2). \tag{8}$$

The Green–Lagrange strain given by Eq. (2) is combined with Eqs. (7)–(8), in order to receive the constitutive relations between the stress components σ_{xz}, σ_{yz} and the displacement w. Thus, the result can be obtained as

$$\sigma_{xz} = \mu\frac{\partial w}{\partial x} + \left(\frac{\mathcal{A}}{4} + \frac{\mathcal{B}}{2}\right)\frac{\partial w}{\partial x}\left(\left(\frac{\partial w}{\partial x}\right)^2 + \left(\frac{\partial w}{\partial y}\right)^2\right) + \left(\frac{3\mathcal{E}}{8} + \frac{\mathcal{F}}{2}\right)\frac{\partial w}{\partial x}\left(\left(\frac{\partial w}{\partial x}\right)^2 + \left(\frac{\partial w}{\partial y}\right)^2\right)^2 + \frac{\mathcal{G}}{2}\frac{\partial w}{\partial x}\left(2\left(\frac{\partial w}{\partial x}\right)^2 + 2\left(\frac{\partial w}{\partial y}\right)^2 + 2\left(\frac{\partial w}{\partial x}\right)^2\left(\frac{\partial w}{\partial y}\right)^2 + \left(\frac{\partial w}{\partial x}\right)^4 + \left(\frac{\partial w}{\partial y}\right)^4\right), \tag{9}$$

$$\sigma_{yz} = \mu\frac{\partial w}{\partial y} + \left(\frac{\mathcal{A}}{4} + \frac{\mathcal{B}}{2}\right)\frac{\partial w}{\partial y}\left(\left(\frac{\partial w}{\partial x}\right)^2 + \left(\frac{\partial w}{\partial y}\right)^2\right) + \left(\frac{3\mathcal{E}}{8} + \frac{\mathcal{F}}{2}\right)\frac{\partial w}{\partial y}\left(\left(\frac{\partial w}{\partial x}\right)^2 + \left(\frac{\partial w}{\partial y}\right)^2\right)^2 + \frac{\mathcal{G}}{2}\frac{\partial w}{\partial y}\left(2\left(\frac{\partial w}{\partial x}\right)^2 + 2\left(\frac{\partial w}{\partial y}\right)^2 + 2\left(\frac{\partial w}{\partial x}\right)^2\left(\frac{\partial w}{\partial y}\right)^2 + \left(\frac{\partial w}{\partial x}\right)^4 + \left(\frac{\partial w}{\partial y}\right)^4\right). \tag{10}$$

One should note that the obtained stress tensor components σ_{xz} and σ_{xz} can be decomposed into linear (superscript L) and nonlinear (superscript NL) terms such that $\sigma_{xz} = \sigma_{xz}^{L} + \sigma_{xz}^{NL}$ and $\sigma_{yz} = \sigma_{yz}^{L} + \sigma_{yz}^{NL}$. For the measure of stress tensor used, the nonlinearity resulting from strain definition is negligible. However, previous works in [34,35] use another definition of stress measure i.e., the first Piola–Kirchhoff stress tensor. In this case the influence of geometric nonlinearity can be observed.

In the absence of body force, Eq. (6) together with the nonlinear stress definitions (9)–(10) lead to the nonlinear homogeneous displacement equation of motion. This equation can be written in a compact form as

$$\frac{\partial^2 w}{\partial x^2} + \frac{\partial^2 w}{\partial y^2} - \frac{1}{c_s^2}\frac{\partial^2 w}{\partial t^2} = -\frac{1}{\mu}\left(\frac{\partial \sigma_{xz}^{NL}}{\partial x} + \frac{\partial \sigma_{yz}^{NL}}{\partial y}\right), \tag{11}$$

where $c_s = \sqrt{\frac{\mu}{\rho}}$ and σ_{xz}^{NL}, σ_{xz}^{NL} are shear wave velocity and nonlinear terms of stress components in Eqs. (9) and (10), respectively. To facilitate further analysis, the linear and nonlinear terms are written on the left-hand and the right-hand side of the equation, respectively. Eqs. (9)–(11) define the analytical model of SH waves in an unbounded nonlinear Landau–Lifshitz medium, which is described by two Lagrangian coordinates x, y and one displacement component w.

2.3. Boundary conditions

The traction vector $\mathbf{t} = \boldsymbol{\sigma}\cdot\mathbf{n} = [t_x,\ t_y,\ t_z]$ is the resultant of stresses acting on a cut surface of arbitrary orientation with the surface outward-pointing normal vector $\mathbf{n}$. For the $2h$-thick semi-infinite plate under consideration and the adopted coordinate system, the normal vectors can be express as $\mathbf{n} = \pm[0, 1, 0]^T$ at $y = \pm h$.

In view of the assumption made in the previous subsection, only the t_z component of traction is considered. Hence, traction-free boundary conditions for propagation of SH guided waves require that

$$t_z = \pm\sigma_{yz} = 0, \text{ for } y = \pm h, \tag{12}$$

where σ_{yz} is defined by Eq. (10). The assumed boundary conditions are nonlinear and homogeneous. For further analysis, the linear and nonlinear terms expressed in Eq. (10) are grouped, and Eq. (12) can be rewritten as

$$\pm\frac{\partial w}{\partial y} = \mp\frac{1}{\mu}\sigma_{yz}^{NL}, \text{ for } y = \pm h. \tag{13}$$

The wave motion Eq. (11) with the boundary conditions given by Eq. (13) formulate a complete mathematical model of SH guided waves propagation problem in a nonlinear hyper-elastic medium. The approximate solution of this nonlinear and homogeneous problem is established in the following section.

3. Perturbation analysis of nonlinear SH guided waves

It is clear that Eq. (11) and associated boundary conditions given by Eq. (13) are nonlinear, therefore an analytical solution cannot be derived. However, the asymptotic approximation of the exact solutions can be obtained via the perturbation analysis [25]. In this work, the multiple-scales technique with the modal decomposition method is used. Such approach for selected nonlinear mechanical systems is presented in [36–38]. This perturbation technique is used to prevent the secular terms in the approximation solution. These secular terms grow infinitely in the fundamental perturbation analysis. This is inconsistent with physical properties of the considered conservative system.

To establish an asymptotic expansion via the multiple scales perturbation method, a small parameter ε needs to be introduced, because none appears explicitly in Eqs. (11) and (13). Also, to eliminate the secular terms, additional time variables are incorporated into the problem as [18,39,40]

$$t_n = \varepsilon^n t, \tag{14}$$

where $n \in \{0,\ 1,\ 2,\ \ldots\}$. Then, the derivatives with respect to t become

$$\frac{\partial}{\partial t} = \frac{\partial}{\partial t_0} + \varepsilon \frac{\partial}{\partial t_1} + \varepsilon^2 \frac{\partial}{\partial t_1} + \cdots, \tag{15}$$

$$\frac{\partial^2}{\partial t^2} = \frac{\partial^2}{\partial t_0^2} + 2\varepsilon \frac{\partial^2}{\partial t_0\, \partial t_1} + \varepsilon^2 \left(\frac{\partial^2}{\partial t_1^2} + 2 \frac{\partial^2}{\partial t_0\, \partial t_2} \right) + \cdots. \tag{16}$$

It is clear that the number of independent time scales required depends on the expansion order. Consequently, the approximate solution of the considered nonlinear SH wave propagation problem can be sought as

$$w(x, y, t_0, t_2, \ldots) = \varepsilon w_1(x, y, t_0, t_2, \ldots) + \varepsilon^3 w_3(x, y, t_0, t_2, \ldots) + \cdots, \tag{17}$$

where the subscripts indicate the order of approximation. Small dimensionless parameter ε is a measure of amplitude of the solution. It can be used as a bookkeeping parameter and set equal to unity if the amplitude is taken to be small as illustrated in [18]. The variable t_0 is the fast time scale and t_2 is the slow time scale, which characterises modulations of the amplitude and phase due to nonlinearity [41].

The slow time variable t_1 and the term w_2 can be omitted in Eq. (17) without loss of generality. This is because the analysed nonlinearity is an odd function of spatial derivatives of the w wavefield [25]. Including the variable t_1 and the term w_2 in the approximate expansion of w leads to equations showing that w is independent of t_1 and w_2 satisfies the same equations as w_1. Hence, the absence of w_2 does not affect the solution.

Upon substitution of Eqs. (16) and (17) into Eqs. (11) and (13), and equating the terms proportional to powers of the parameter ε to zero, the governing equations and associated boundary conditions for the first and third order of approximation are defined by

$$O(\varepsilon) : \frac{\partial^2 w_1}{\partial x^2} + \frac{\partial^2 w_1}{\partial y^2} - \frac{1}{c_s^2} \frac{\partial^2 w_1}{\partial t_0^2} = 0, \tag{18}$$

$$O(\varepsilon) : \pm \frac{\partial w_1}{\partial y} = 0, \text{ for } y = \pm h, \tag{19}$$

$$\begin{aligned} O(\varepsilon^3) : \frac{\partial^2 w_3}{\partial x^2} + \frac{\partial^2 w_3}{\partial y^2} - \frac{1}{c_s^2} \frac{\partial^2 w_3}{\partial t_0^2} &= \frac{2}{c_s^2} \frac{\partial^2 w_1}{\partial t_0\, \partial t_2} - \frac{1}{\mu} \left(\frac{\partial (\sigma_{xz}^{NL})_1}{\partial x} + \frac{\partial (\sigma_{yz}^{NL})_1}{\partial y} \right) \\ &= \frac{2}{c_s^2} \frac{\partial^2 w_1}{\partial t_0\, \partial t_2} - \frac{1}{\mu} \left(\frac{\mathcal{A}}{4} + \frac{\mathcal{B}}{2} + \mathcal{C} \right) \left[\frac{\partial}{\partial x} \left(\frac{\partial w_1}{\partial x} \left(\left(\frac{\partial w_1}{\partial x} \right)^2 + \left(\frac{\partial w_1}{\partial y} \right)^2 \right) \right) + \frac{\partial}{\partial y} \left(\frac{\partial w_1}{\partial y} \left(\left(\frac{\partial w_1}{\partial x} \right)^2 + \left(\frac{\partial w_1}{\partial y} \right)^2 \right) \right) \right], \end{aligned} \tag{20}$$

$$O(\varepsilon^3) : \pm \frac{\partial w_3}{\partial y} = \mp \frac{1}{\mu} (\sigma_{yz}^{NL})_1 = \mp \frac{1}{\mu} \left(\frac{\mathcal{A}}{4} + \frac{\mathcal{B}}{2} + \mathcal{C} \right) \frac{\partial w_1}{\partial y} \left(\left(\frac{\partial w_1}{\partial x} \right)^2 + \left(\frac{\partial w_1}{\partial y} \right)^2 \right), \text{ for } y = \pm h. \tag{21}$$

The terms $(\sigma_{xz}^{NL})_1$, $(\sigma_{yz}^{NL})_1$ in Eqs. (20)–(21) are nonlinear parts of stress tensor components σ_{xz}, σ_{yz} – defined by Eqs. (9)–(10) – for the first order approximation solution w_1.

It is important to note at this point that the nonlinear homogeneous problem of SH guided wave propagation in a hyperelastic material (described by Eqs. (11) and (13)) reduces to the system of linear partial differential equations with the corresponding linear boundary conditions. The linear differential operators acting on w_1 and w_3 on the left-hand side are identical. This conclusion holds for higher order approximations. The nonlinear forcing terms on the right-hand side of the analysed equations can be interpreted as an excitation of the higher order approximation by the lower order approximation of the wavefield and depends on the definition of nonlinearity. Therefore, the problems defined by Eqs. (18)–(21) must be solved recursively. Different approaches have been proposed to tackle this problem. In what follows, the multiple-scale perturbation method together with the normal mode decomposition approach [36,38] is used to determine the solution in terms of the nonlinear normal-mode manifold.

3.1. First order approximation

The homogeneous Eq. (18) with the associated boundary conditions given by Eq. (19) can be solved via the separation of variables method. Thus, the solution of this equation is assumed to be a product of two functions [42]

$$w_1(x, y, t_0, t_2) = Y(y) A_1(x, t_0, t_2). \tag{22}$$

The $Y(y)$ function needs to satisfy the boundary conditions and the $A(x, t_0, t_2)$ function describes the distribution of SH guided wave in time and space. This assumption leads to the eigenvalue problem defined as

$$Y(y)'' + \eta^2 Y(y) = 0, \tag{23}$$

$$\pm \frac{\partial Y(y)}{\partial y} = 0, \text{ for } y = \pm h, \tag{24}$$

and the equation for the amplitude distribution along x direction and evolution in time of $A_1(x, t_0, t_2)$ is

$$\frac{\partial^2 A_1}{\partial x^2} - \eta^2 A_1 - \frac{1}{c_s^2} \frac{\partial^2 A_1}{\partial t_0^2} = 0. \tag{25}$$

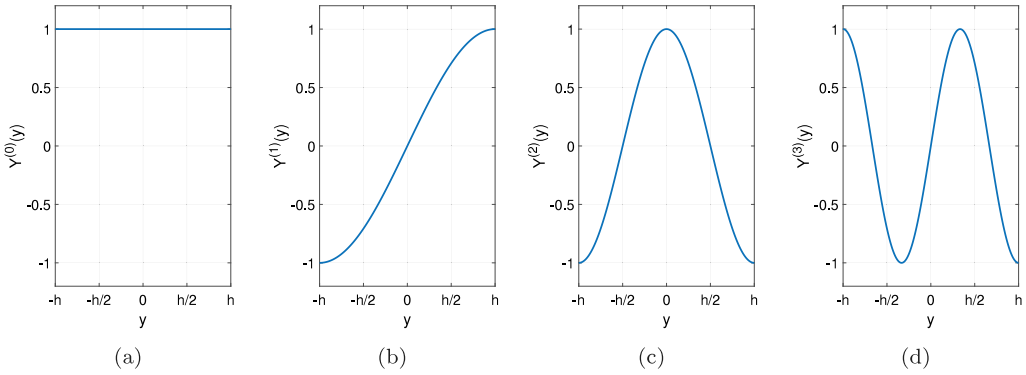

Fig. 2. Selected eigenfunctions for SH guided waves: (a) SH0 mode-shape (b) SH1 mode-shape (c) SH2 mode-shape (d) SH3 mode-shape.

The solution of Eqs. (23) and (24) yields an infinite set $\{\eta_m^2\}$ of distinctive eigenvalues, which are associated with a set of $\{Y^{(m)}(y)\}$ characteristics functions, where $m \in \{0,\ 1,\ 2,\ \ldots\}$. These functions are known in mathematics as eigenfunctions and physically can be recognised as natural modes. If these functions are normalised, thus providing their amplitudes unique, then they are called normal modes [43]. One can show that the considered eigenvalue problem is self-adjoint [42]. Therefore, the eigenvalues are real and non-negative. Moreover, the eigenfunctions are orthogonal and form a complete set of functions.

For the considered problem, the eigenvalues can be expressed as $\eta_m^2 = (m\frac{\pi}{2h})^2$. The $\{Y^{(m)}(y)\}$ eigenfunction set can be dived into two subsets i.e. the symmetric $\{Y_S^{(i)}(y)\}$ and the antisymmetric $\{Y_A^{(i)}(y)\}$ modes for SH guided waves given as

$$Y_S^{(i)}(y) = \cos(\eta_{2i}y), \tag{26}$$

$$Y_A^{(i)}(y) = \sin(\eta_{2i+1}y), \tag{27}$$

where $i \in \{0,\ 1,\ 2,\ \ldots\}$. Selected eigenfunctions are presented in Fig. 2.

For each $Y^{(m)}(y)$, there is a function $A_1^{(m)}(x, t_0, t_2)$, which is the solution of Eq. (25) with $\eta = \eta_m$. The equation describing evolution of the amplitude of the m-th mode for first order approximation is referred in the literature [24] as the Klein–Gordon equation, for which the dispersion relation is

$$\frac{\omega^2}{c_s^2} = \eta_m^2 + \xi^2, \tag{28}$$

where ω is angular frequency and ξ is a wavenumber. For m = 0, the angular frequency and wave number are linearly dependent and differential Eq. (25) is reduced to the wave equation for bulk waves. This means that the SH0 mode is non-dispersive.

The above considerations lead to the general first order solution in the following form

$$\begin{aligned} w_1(x, y, t_0, t_2) &= \sum_{m=0}^{\infty} Y^{(m)}(y) A_1^{(m)}(x, t_0, t_2) \\ &= \sum_{i=0}^{\infty} Y_S^{(i)}(y) A_1^{(2i)}(x, t_0, t_2) + \sum_{i=0}^{\infty} Y_A^{(i)}(y) A_1^{(2i+1)}(x, t_0, t_2). \end{aligned} \tag{29}$$

The obtained solution recovers the classical linear SH guided wave propagation problem.

This study investigates the influence of the assumed material nonlinearity on the dispersion characteristics and the higher-order displacement field corresponding to SH guided waves in the $2h$-thick plate. Therefore, it is assumed that in the considered system the steady-state harmonic displacement field – corresponding to the dominant m_0-th mode propagating in the positive x-axis direction – is excited. For the considered problem, the resonances occur between an infinite number of linear SH modes [22]. All SH modes that are involved in the internal resonances and propagate in the positive x-axis direction should be considered in the first order approximation w_1. Hence, the first order approximation solution, when dominant m_0 mode is dispersive, is assumed in the form

$$w_1(x, y, t_0, t_2) = \sum_r \vartheta^r Y^{(rm_0)}(y) \alpha_1^{(rm_0)}(t_2) e^{ir(\xi_0 x - \omega_0 t_0)} + c.c., \tag{30}$$

where c.c. stands for the complex conjugate of all preceding terms and $r \in \{1,\ 3,\ \ldots\}$. The index r belongs to a set of odd numbers due to the form of the assumed nonlinearity. The m_0-th SH mode is the driving mode, which can be excited directly in a structure with frequency and wavenumber satisfying the dispersion relation (28) and equal to ξ_0 and ω_0, respectively. The higher order modes (odd multiplies of m_0) can be regarded as companion modes, which exist because of the internal resonances.

The coefficient $\alpha_1^{(rm_0)}(t_2)$ is the complex amplitude of the rm_0-th SH mode and $\vartheta \ll 1$ is a dimensionless parameter. The amplitude $\alpha_1^{(rm_0)}(t_2)$ is determined to prevent the secular terms. The purpose of entering the parameter ϑ is to indicate the range of amplitude of each propagating mode, by arranging the forcing terms in a descending order. For $m_0 = 0$ (driving mode is the nondispersive SH0)

the distribution along y direction of first order approximation reduces to the SH0 linear mode shape. This is because this mode is in inter-resonance only with itself for the modelled material nonlinearity. For this case, the first approximate solution can be expressed as

$$w_1(x,y,t_0,t_2) = Y^{(0)}(y)\sum_r \vartheta^r \alpha_1^{(r)}(t_2) e^{ir(\xi_0 x-\omega_0 t_0)} + c.c. \tag{31}$$

The considered first order SH guided wave problem defined by Eqs. (18) and (19) - recovers the classical SH guided wave propagation problem in a linear plate. The steady-state harmonic solution for the first order homogeneous problem is equal to the sum of harmonic waves with the angular frequency–wavenumber pairs (ω,ξ) resulting from dispersion relations for each mode separately. The through-thickness profiles for each of these waves correspond to SH mode shapes. These mode shapes – eigenfunctions for SH guided waves problem – are orthogonal and form a complete set of functions. Therefore, they are used to solve inhomogeneous problem defined by Eqs. (20) and (21).

3.2. Third order approximation

The mathematical model given by Eqs. (20) and (21) defines the inhomogeneous SH guided wave problem. The forcing terms, which depend on the first order solution given by Eq. (30), cannot be obtained arbitrary and the multiple scale technique allows one to remove the nonphysical secular terms. In this section, two special cases for the first order solutions and their effect on higher order solutions are considered. For the first one, only the dispersive modes will be studied. In the second one, the SH0 mode will be analysed separately due to its nondispersive properties.

3.2.1. Third order approximation for dispersive modes

The problem defined by Eqs. (20) and (21) is linear and inhomogeneous. The forcing terms in boundary conditions can be interpreted as external forces at the system boundaries. To find the solution using the modal analysis eigenfunctions expansion method, firstly the boundary conditions must be homogenised. This can be realised using the properties of the Dirac delta function, as illustrated in [44]. Eq. (20) can be rewritten with homogeneous boundary conditions as

$$\frac{\partial^2 w_3}{\partial x^2}+\frac{\partial^2 w_3}{\partial y^2}-\frac{1}{c_s^2}\frac{\partial^2 w_3}{\partial t_0^2} = \frac{2}{c_s^2}\frac{\partial^2 w_1}{\partial t_0\,\partial t_2}-\frac{1}{\mu}\left(\frac{\partial(\sigma_{xz}^{NL})_1}{\partial x}+\frac{\partial(\sigma_{yz}^{NL})_1}{\partial y}-\delta(y-h)(\sigma_{yz}^{NL})_1+\delta(y+h)(\sigma_{yz}^{NL})_1\right), \tag{32}$$

$$\pm\frac{\partial w_3}{\partial y}=0,\ \text{for } y=\pm h. \tag{33}$$

The solution of Eqs. (32) and (33) can be expressed as

$$w_3(x,y,t_0,t_2)=\sum_{m=0}^{\infty} Y^{(m)}(y)A_3^{(m)}(x,t_0,t_2), \tag{34}$$

where the $Y^{(m)}(y)$ eigenfunctions – satisfying homogeneous boundary conditions – are known, while the $A^{(m)}(x,t_0,t_2)$ amplitudes must be determined. To shorten the notation, the f_1^{NL} term is introduced, which corresponds to the space-distributed forcing term and is defined as follows

$$f_1^{NL}=\frac{\partial(\sigma_{xz}^{NL})_1}{\partial x}+\frac{\partial(\sigma_{yz}^{NL})_1}{\partial y}. \tag{35}$$

Upon substitution of Eq. (34) into Eq. (32) the following governing equation is obtained

$$\sum_{m=0}^{\infty} Y^{(m)}\frac{\partial^2 A_3^{(m)}}{\partial x^2}+\sum_{m=0}^{\infty} Y^{(m)\prime\prime}A_3^{(m)}-\frac{1}{c_s^2}\sum_{m=0}^{\infty} Y^{(m)}\frac{\partial^2 A_3^{(m)}}{\partial t_0^2}=\frac{2}{c_s^2}\frac{\partial^2 w_1}{\partial t_0\,\partial t_2}-\frac{1}{\mu}\left(f_1^{NL}-\delta(y-h)(\sigma_{yz}^{NL})_1+\delta(y+h)(\sigma_{yz}^{NL})_1\right). \tag{36}$$

The definition of the forcing term f_1^{NL} results from Eq. (35). The second derivative of $Y^{(m)\prime\prime}(y)$ should be removed, so Eq. (23) is used and the equation under consideration can be rewritten in the form

$$\sum_{m=0}^{\infty} Y^{(m)}\left(\frac{\partial^2 A_3^{(m)}}{\partial x^2}-\eta_m^2 A_3^{(m)}-\frac{1}{c_s^2}\frac{\partial^2 A_3^{(m)}}{\partial t_0^2}\right)=\frac{2}{c_s^2}\frac{\partial^2 w_1}{\partial t_0\,\partial t_2}-\frac{1}{\mu}\left(f_1^{NL}-\delta(y-h)(\sigma_{yz}^{NL})_1+\delta(y+h)(\sigma_{yz}^{NL})_1\right). \tag{37}$$

Before any further analyses, f_1^{NL} can be expanded in series with the base defined by a set of functions $\{Y^{(m)}(y)\}$

$$f_1^{NL}=\vartheta^3\sum_{r=1,3}Y^{(rm_0)}\sum_{k=1,3}C_{(1,\vartheta^3)}^{(rm_0,k)}e^{ik(\xi_0 x-\omega_0 t_0)}+\vartheta^5\sum_{r=1,3,5}Y^{(rm_0)}\sum_{k=1,3,5}C_{(1,\vartheta^5)}^{(rm_0,k)}e^{ik(\xi_0 x-\omega_0 t_0)}+\cdots+c.c., \tag{38}$$

where coefficients $C_{(1,\vartheta^3)}^{(rm_0,k)}$, $C_{(1,\vartheta^5)}^{(rm_0,k)}$, … depend on set $\{\alpha_1^{(rm_0)}(t_2)\}$ of complex amplitudes. Multiplying Eq. (37) by $Y^{(m)}(y)$ and integrating over the y variable in the $\langle -h,\ h\rangle$ interval and invoking the orthogonality conditions gives an infinite number of equations for each mode amplitude $A_3^{(m)}(x,y,t_0,t_2)$, i.e.

$$\frac{\partial^2 A_3^{(m)}}{\partial x^2}-\eta_m^2 A_3^{(m)}-\frac{1}{c_s^2}\frac{\partial^2 A_3^{(m)}}{\partial t_0^2}=\frac{\int_{-h}^{h}(\frac{2}{c_s^2}\frac{\partial^2 w_1}{\partial t_0\,\partial t_2}-\frac{1}{\mu}f_1^{NL})Y^{(m)}(y)dy}{\int_{-h}^{h}(Y^{(m)}(y))^2 dy}. \tag{39}$$

In this particular case, the property of the Dirac delta function and boundary conditions for the solution of the first order Eq. (19), namely $\pm\frac{\partial^2 w_1}{\partial y^2} = 0$ for $y = \pm h$, leads to the absence of the external forces that result from the boundary conditions for each mode amplitude. In general, these excitation terms, which result from forcing at the borders, are not equal to zero.

After substituting the series from Eqs. (30) and (38) into Eq. (39), one can observe that only the equations for amplitudes, corresponding to modes: m_0, $3m_0$, $5m_0, \ldots$ are inhomogeneous. Therefore, the expansion of the third order approximation $w_3(x, t_1, t_2)$ from Eq. (34) contains only terms with numbers equal to odd multiplies of m_0; similarly, as the first order solution $w_1(x, t_1, t_2)$ from Eq. (29). The first three nonhomogeneous equations from Eq. (39) are given by

$$\frac{\partial^2 A_3^{(m_0)}}{\partial x^2} - \eta_{m_0}^2 A_3^{(m_0)} - \frac{1}{c_s^2}\frac{\partial^2 A_3^{(m_0)}}{\partial t_0^2} = -i\omega_0\vartheta\frac{2}{c_s^2}\frac{\partial \alpha_1^{(m_0)}}{\partial t_2}e^{i(\xi_0 x-\omega_0 t_0)} - \frac{1}{\mu}\left(\vartheta^3\sum_{k=1,3} C_{(1,\vartheta^3)}^{(m_0,k)} e^{ik(\xi_0 x-\omega_0 t_0)} + \cdots\right) + c.c., \tag{40}$$

$$\frac{\partial^2 A_3^{(3m_0)}}{\partial x^2} - \eta_{3m_0}^2 A_3^{(3m_0)} - \frac{1}{c_s^2}\frac{\partial^2 A_3^{(3m_0)}}{\partial t_0^2} = -i3\omega_0\vartheta^3\frac{2}{c_s^2}\frac{\partial \alpha_1^{(3m_0)}}{\partial t_2}e^{i3(\xi_0 x-\omega_0 t_0)} - \frac{1}{\mu}\left(\vartheta^3\sum_{k=1,3} C_{(1,\vartheta^3)}^{(3m_0,k)} e^{ik(\xi_0 x-\omega_0 t_0)} + \cdots\right) + c.c., \tag{41}$$

$$\frac{\partial^2 A_3^{(5m_0)}}{\partial x^2} - \eta_{5m_0}^2 A_3^{(5m_0)} - \frac{1}{c_s^2}\frac{\partial^2 A_3^{(5m_0)}}{\partial t_0^2} = -i5\omega_0\vartheta^5\frac{2}{c_s^2}\frac{\partial \alpha_1^{(5m_0)}}{\partial t_2}e^{i5(\xi_0 x-\omega_0 t_0)} - \frac{1}{\mu}\left(\vartheta^5\sum_{k=1,3,5} C_{(1,\vartheta^5)}^{(5m_0,k)} e^{ik(\xi_0 x-\omega_0 t_0)} + \cdots\right) + c.c. \tag{42}$$

All terms are ranked in descending order defined by ϑ in the right-hand side of the above equations. Moreover, these equations contain terms that produce non-physical results. These terms are proportional to $e^{ir(\xi_0 x-\omega_0 t_0)}$ for every $A_3^{(rm_0)}$ amplitude and should be removed. In general, for each analysed equation there exists an infinite number of these terms proportional to successive odd powers of ϑ. To remove all these components, it is necessary to solve an infinite number of coupled differential equations and determine the set of functions of the slow time variable $\{\alpha_1^{(rm_0)}(t_2)\}$. This process is tedious or even impossible in an analytical way. The more the forcing terms proportional to successive powers of the parameter ϑ are taken into account, the more accurate the solution will be, but the number of calculations will drastically increase.

To prevent the secular terms, it is required that the $\{\alpha_1^{(rm_0)}(t_2)\}$ set of amplitude be a solution of the set of infinite number of ordinary differential equations defined as

$$-i\omega_0\vartheta\frac{2}{c_s^2}\frac{\partial \alpha_1^{(m_0)}}{\partial t_2} - \frac{1}{\mu}\vartheta^3 C_{(1,\vartheta^3)}^{(m_0,1)} + \cdots = 0, \tag{43}$$

$$-i3\omega_0\vartheta^3\frac{2}{c_s^2}\frac{\partial \alpha_1^{(3m_0)}}{\partial t_2} - \frac{1}{\mu}\vartheta^3 C_{(1,\vartheta^3)}^{(3m_0,3)} + \cdots = 0, \tag{44}$$

$$-i5\omega_0\vartheta^5\frac{2}{c_s^2}\frac{\partial \alpha_1^{(5m_0)}}{\partial t_2} - \frac{1}{\mu}\vartheta^5 C_{(1,\vartheta^5)}^{(5m_0,5)} + \cdots = 0. \tag{45}$$

Here, the study is limited to solving only Eq. (43) with the omission of the terms proportional to ϑ^5 and higher powers of this parameter. The complex solution of this equation where

$$C_{(1,\vartheta^3)}^{(m_0,1)} = -\frac{1}{4}\left(\frac{\mathcal{A}}{4} + \frac{\mathcal{B}}{2} + \mathcal{G}\right)(9\eta_{m_0}^4 + 2\eta_{m_0}^2\xi_0^2 + 9\xi_0^4)(\alpha_1^{(m_0)})^2\overline{\alpha_1^{(m_0)}}, \tag{46}$$

can be expressed in an exponential form as

$$\alpha_1^{(m_0)}(t_2) = \frac{1}{2}\beta^{(m_0)}(t_2)e^{i\gamma^{(m_0)}(t_2)}, \tag{47}$$

where $\beta^{(m_0)}(t_2)$ and $\gamma^{(m_0)}(t_2)$ are real. The over-lined part in Eq. (46) represents the complex conjugate. Eq. (43), after separating real and imaginary parts and omitting small terms, yields

$$\begin{aligned}\frac{\partial \beta^{(m_0)}}{\partial t_2} &\simeq 0,\\ \frac{\partial \gamma^{(m_0)}}{\partial t_2} &\simeq -\frac{\vartheta^2 c_s^2}{32\mu\omega_0}\left(\frac{\mathcal{A}}{4} + \frac{\mathcal{B}}{2} + \mathcal{G}\right)(9\eta_{m_0}^4 + 2\eta_{m_0}^2\xi_0^2 + 9\xi_0^4)(\beta^{(m_0)})^2.\end{aligned} \tag{48}$$

It follows from Eq. (48) that $\beta^{(m_0)}$ is equal to an arbitrary constant and this leads to the solution

$$\beta^{(m_0)} \simeq \beta_0^{(m_0)}, \tag{49}$$

$$\gamma^{(m_0)} \simeq -\frac{\vartheta^2 c_s^2}{32\mu\omega_0}\left(\frac{\mathcal{A}}{4} + \frac{\mathcal{B}}{2} + \mathcal{G}\right)(9\eta_{m_0}^4 + 2\eta_{m_0}^2\xi_0^2 + 9\xi_0^4)(\beta_0^{(m_0)})^2 t_2 + \gamma_0^{(m_0)}, \tag{50}$$

where $\beta_0^{(m_0)}$ and $\gamma_0^{(m_0)}$ are integration constants. Eqs. (49)–(50) yield

$$\alpha_1^{(m_0)}(t_2) \simeq \beta_0^{(m_0)} e^{i\left(-\frac{\vartheta^2 c_s^2}{32\mu\omega_0}\left(\frac{\mathcal{A}}{4}+\frac{\mathcal{B}}{2}+\mathcal{G}\right)(9\eta_{m_0}^4+2\eta_{m_0}^2\xi_0^2+9\xi_0^4)(\beta_0^{(m_0)})^2 t_2+\gamma_0^{(m_0)}\right)}. \tag{51}$$

From Eq. (51) results that the amplitude of the dominant m_0 SH mode in first order approximation solution for the considered nonlinear problem is periodic. Hence the periodic wave-trains for this mode are possible in a nonlinear system.

The dispersion relation for the m_0 SH mode, obtained using Eqs. (30) and (51), is given by

$$\omega_{m_0}(\xi_0,\beta_0^{(m_0)}) = \omega_0 + \varepsilon\omega_1 + \varepsilon^2\omega_2 + \cdots = \omega_0 + \varepsilon^2 \frac{\vartheta^2 c_s}{32\mu\sqrt{\xi_0^2+\eta_{m_0}^2}}\left(\frac{\mathcal{A}}{4}+\frac{\mathcal{B}}{2}+\mathcal{G}\right)(9\eta_{m_0}^4 + 2\eta_{m_0}^2\xi_0^2 + 9\xi_0^4)(\beta_0^{(m_0)})^2 + \cdots, \tag{52}$$

where $\omega_0 = c_s\sqrt{\xi_0^2+\eta_{m_0}^2}$. Eq. (52) shows that the frequency shift is a function of wavenumber. This function is approximately constant for wavenumbers smaller than the considered eigenvalue η_{m_0}. For wavenumbers bigger than this eigenvalue, the frequency shift can be approximated by cubic function.

It is important to note that the angular frequency shift of the dispersion curve – for the dominant m_0-th SH mode – depends on the amplitude parameter $\beta_0^{(m_0)}$, and the elastic constants $\mathcal{A}$, $\mathcal{B}$, $\mathcal{G}$. Sequentially, performing further calculations, taking into account the most significant forcing terms will allow one to determine the shifts of dispersion curves for higher modes generated due to the existence of material nonlinearity.

Coefficients $C_{(1,\vartheta^3)}^{(rm_0,k)}$, $C_{(1,\vartheta^5)}^{(rm_0,k)}$, ... in Eqs. (43)–(45) tends to zero as nonlinear material parameters vanish. For this case, the integration constants can be assumed in such a manner that the amplitudes $\alpha_1^{(rm_0)}(t_2)$ of all – except the m_0 SH mode – are equal to zero. Consequently, if material nonlinear constants are equal to zero, the m_0 SH mode only exists in the considered system.

The solution of the third order problem – defined by Eqs. (20) and (21) – is equal to a double series

$$w_3(x,y,t_0,t_2) = \sum_r Y^{(rm_0)} \sum_k \alpha_2^{(rm_0,k)}(t_2) e^{ik(\xi_0 x - \omega_0 t_0)} + c.c., \tag{53}$$

where r, k $\in \{1, 3, \ldots\}$ and for $r = k$ the amplitude $\alpha_2^{(rm_0,k)}$ is equal to zero. This results from preventing the secular terms. This notation means that the third order displacement field w_3 is a sum of an infinite number of harmonic waves which are in general amplitude modulated. The phenomenon of modulation of individual waves is characterised by a slow time variable t_2. The distribution of the wavefield along the y axis is a sum of an infinite number of eigenfunctions $Y^{(rm_0)}(y)$ multiplied by their respective amplitudes.

The amplitudes $\alpha_2^{(rm_0,k)}(t_2)$ should be determined using calculations performed for the fifth-order approximation and the removal of the secular components of the solution.

3.2.2. Third order approximation for the non-dispersive SH0 mode

This subsection presents the case for which the first order approximation contains only the linear SH0 mode. It is possible to carry out analogous reasoning to that presented in the previous subsection. Namely, the form of the first order approximation is considered as

$$w_1(x,y,t_0,t_2) = Y^{(0)}(y) \sum_r \vartheta^r \alpha_1^{(r)}(t_2) e^{ir(\xi_0 x - \omega_0 t_0)} + c.c. \tag{54}$$

Then this relationship, after inserting into Eq. (20) yields as before Eqs. (32) and (33). Due to the form of the function $Y^{(0)}(y)$ and the definition of σ_{yz} from Eq. (10), the term $(\sigma_{yz}^{NL})_1$ in Eq. (32) is equal to zero. The solution of this equation can be assumed as before in the form Eq. (34). For the first order approximation defined in Eq. (54), the right-hand side of Eq. (37) is non-orthogonal only with function $Y^{(0)}(y)$. This means that all equations corresponding to $A^{(m)}(x,t_0,t_2)$ are homogeneous and their solution is trivial, except for m = 0. The only inhomogeneous equation is given by

$$\frac{\partial^2 A_3^{(0)}}{\partial x^2} - \frac{1}{c_s^2}\frac{\partial^2 A_3^{(0)}}{\partial t_0^2} = \frac{\int_{-h}^{h}\left(\frac{2}{c_s^2}\frac{\partial^2 w_1}{\partial t_0\,\partial t_2} - \frac{1}{\mu}f_1^{NL}\right)Y^{(0)}(y)\,dy}{\int_{-h}^{h}(Y^{(0)}(y))^2\,dy}, \tag{55}$$

where f_1^{NL} is defined in Eq. (38). After inserting the relationship from Eqs. (54) to (55), this can be rewritten in the form

$$\frac{\partial^2 A_3^{(0)}}{\partial x^2} - \frac{1}{c_s^2}\frac{\partial^2 A_3^{(0)}}{\partial t_0^2} = -i\frac{2\omega_0}{c_s^2}\sum_r r\vartheta^r \frac{\partial \alpha_1^{(r)}}{\partial t_2} e^{ir(\xi_0 x - \omega_0 t_0)} - \frac{1}{\mu}\left(\vartheta^3 \sum_k C_{(1,\vartheta^3)}^{(0,k)} e^{ik(\xi_0 x - \omega_0 t_0)} + \cdots\right) + c.c. \tag{56}$$

One can observe that every term proportional to successive powers of $e^{i(\xi_0 x - \omega_0 t_0)}$ contributes to the generation of the non-physical secular terms. In order that the third order approximation is bounded, all these terms must be removed [18]. To prevent the secular terms, it is required that the set of amplitudes $\{\alpha_1^{(r)}(t_2)\}$ is a solution of the set of infinite number of ordinary differential equations. The system of differential equations can be arranged analogous to that defined for dispersive modes. The first three equations are the same as those from Eqs. (43) and (44). By performing further calculations, it is possible to determine the individual amplitudes $\alpha_1^{(r)}(t_2)$. As a result the third order approximation is a solution of homogeneous differential equation. This solution is analogous to the solution of Eq. (31), i.e. it contains only the SH0 mode. For this case the solution of Eq. (43) with the coefficient defined as

$$C_{(1,\vartheta^3)}^{(0,1)} = -3\left(\frac{\mathcal{A}}{4}+\frac{\mathcal{B}}{2}+\mathcal{G}\right)\xi_0^4(\alpha_1^{(1)})^2\overline{\alpha_1^{(1)}}, \tag{57}$$

can be written as

$$\alpha_1^{(1)}(t_2) \simeq \beta_0^{(1)} e^{i\left(-\frac{3\vartheta^2 c_s^2}{8\mu\omega_0}\left(\frac{\mathcal{A}}{4}+\frac{\mathcal{B}}{2}+\mathcal{G}\right)\xi_0^4(\beta_0^{(1)})^2 t_2 + \gamma_0^{(1)}\right)}. \tag{58}$$

Hence, the amplitude of the dominant SH0 mode in first order approximation solution for the considered nonlinear problem is periodic. Based on Eqs. (31) and (58) the dispersion relation for the first harmonic of SH0 mode depends on its amplitude and is given by

$$\omega_{SH0}(\xi_0,\beta_0^{(1)}) = \omega_0 + \varepsilon\omega_1 + \varepsilon^2\omega_2 + \cdots = \omega_0 + \varepsilon^2\frac{3\vartheta^2 c_s}{8\mu}\left(\frac{\mathcal{A}}{4} + \frac{\mathcal{B}}{2} + \mathcal{C}\right)\xi_0^3(\beta_0^{(1)})^2 + \cdots, \tag{59}$$

where $\omega_0 = c_s\xi_0$. Eq. (59) shows that frequency shift for the nondispersive SH0 mode is a cubic function of wavenumber.

Interestingly, the approach used in this section – to obtain the approximate solution for the SH0 mode – can be also applied for the analysis of shear bulk waves.

3.3. Discussion

This section discusses the approximate solutions – obtained in Sections 3.1 and 3.2 – in a broader context of nonlinear modes. The general approximate solution – expressed by Eq. (17) – for the problem of SH guided wave propagation in nonlinear material – for the case with the dominant dispersive m_0 mode – is given by Eqs. (30) and (53) for the first and third order of approximation, respectively. This general solution can be re-written for the m_0 mode as

$$w(x,y,t_0,t_2) = \varepsilon\sum_{r=1,3,5,\ldots}\vartheta^r Y^{(rm_0)}\alpha_1^{(rm_0)}(t_2)e^{ir(\xi_0 x-\omega_0 t_0)} + \varepsilon^3\sum_{r=1,3,5,\ldots}Y^{(rm_0)}\sum_{k=1,3,5,\ldots}\alpha_2^{(rm_0,k)}(t_2)e^{ik(\xi_0 x-\omega_0 t_0)} + c.c., \tag{60}$$

where for r = k the amplitude $\alpha_2^{(rm_0,k)}$ is equal to zero. Thus, the steady-state harmonic solution for the first order homogeneous problem is equal to the sum of harmonic waves with angular frequencies – i.e., wavenumber pairs $(\omega,\xi) = (r\omega_0, r\xi_0)$ – resulting from dispersion relations for each mode separately. The through-thickness profiles for each of these waves correspond to linear SH mode shapes. This first-order approximation is the sum of modes that are in inner resonances. This approximate solution can be rewritten in the form

$$\begin{aligned} w(x,y,t_0,t_2) = {} & \varepsilon Y^{(m_0)}\vartheta\alpha_1^{(m_0)}(t_2)e^{i(\xi_0 x-\omega_0 t_0)} \\ & + \varepsilon\sum_{r=3,5,\ldots}\vartheta^r Y^{(rm_0)}\alpha_1^{(rm_0)}(t_2)e^{ir(\xi_0 x-\omega_0 t_0)} + \varepsilon^3\sum_{r=1,3,5,\ldots}Y^{(rm_0)}\sum_{k=1,3,5,\ldots}\alpha_2^{(rm_0,k)}(t_2)e^{ik(\xi_0 x-\omega_0 t_0)} + c.c. \end{aligned} \tag{61}$$

One should note that the modal decomposition method has been used to determine the first and third order approximations. In consequence, the contributions of particular mode shape and higher harmonics to the resulting displacement field have been determined. The solution given by Eq. (61) (i.e., the resulting wavefield described by the first and third order approximations) can be interpreted as a nonlinear m_0 mode, by analogy with nonlinear vibration analysis in [37]. The first term in Eq. (60) represents the wavefield for the dominant m_0 SH mode in linear material and the other terms can be interpreted as the nonlinear distortion of the wavefield. The latter tends to zero as nonlinear parameters vanish. The concept of nonlinear vibration modes has been originally proposed in the mid-1960s [45] and then followed in a series of articles on nonlinear discrete and continuous vibration systems [36,38,46,47].

The approximate solution of considered nonlinear problem of SH guided waves propagation, for the case with the dominant nondispersive $m_0 = 0$ mode, can be written in the form

$$w(x,y,t_0,t_2) = \varepsilon Y^{(0)}\sum_{r=1,3,5,\ldots}\vartheta^r\alpha_1^{(r)}(t_2)e^{ir(\xi_0 x-\omega_0 t_0)} + \varepsilon^3 Y^{(0)}\sum_{r=1,3,5,\ldots}\alpha_2^{(r)}(t_2)e^{ir(\xi_0 x-\omega_0 t_0)} + c.c. \tag{62}$$

Similarly, to the previous case discussed, the steady-state harmonic solution for the first order homogeneous problem is equal to the sum of harmonic waves with angular frequency–wavenumber pairs resulting from dispersion relations for $m_0 = 0$ SH mode. The through-thickness profiles for each of these waves correspond to the same SH0 mode shapes. This first-order approximation is the sum of modes that are in inner resonances. The obtained solution for this case also can be interpreted as a nonlinear SH0 mode [37]. One can notice that the wavefield for this case is distorted only alongside the x-axis, because odd higher harmonics are generated. The obtained approximate solution for this case can be rewritten in the form

$$\begin{aligned} w(x,y,t_0,t_2) = {} & \varepsilon Y^{(0)}\vartheta\alpha_1^{(1)}(t_2)e^{i(\xi_0 x-\omega_0 t_0)} \\ & + \varepsilon Y^{(0)}\sum_{r=3,5,\ldots}\vartheta^r\alpha_1^{(r)}(t_2)e^{ir(\xi_0 x-\omega_0 t_0)} + \varepsilon^3 Y^{(0)}\sum_{r=1,3,5,\ldots}\alpha_2^{(r)}(t_2)e^{ir(\xi_0 x-\omega_0 t_0)} + c.c. \end{aligned} \tag{63}$$

The first term in the above equation represents the wavefield for the dominant SH0 mode in linear material and the other terms can be interpreted as the nonlinear distortion of the wavefield, which tends to zero as nonlinear parameters vanish.

Vibration analysis on nonlinear modes described in [36,37] presents an equation that governs the third-order contribution of all modes – other than the nth linear mode – to the nth nonlinear mode, for a nonlinear system. In this paper, the contribution of each rm_0-th SH mode shape on nonlinear SH modes – for both investigated cases – results from Eqs. (61) and (63). The first term in the sums of these equations corresponds to the linear wavefield, whereas the other terms can be interpreted as mode distortion. The amplitudes α - that depend on slow time t_2 - are measures of contribution of each SH linear mode shape and generated higher harmonics on the approximate solution.

For the assumed value of x coordinate, all particles of considered medium for the first and third approximate solutions execute motion with the same period, i.e., pass through their static equilibrium and achieve their maximum displacements at the same

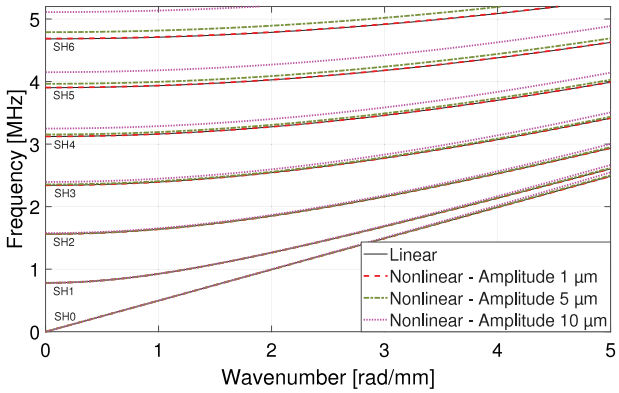

Fig. 3. Linear and nonlinear analytical dispersion curves for dominant SH modes (Eqs. (52) and (59)) in a 2 mm thick aluminium plate for selected amplitudes. The scale factor for component ω_2 is equal to 10.

Table 1
Material properties (in GPa) of aluminium used in nonlinear SH wave propagation simulations.

λ	μ	$\mathcal{A}$	$\mathcal{B}$	$\mathcal{C}$	$\mathcal{E}$	$\mathcal{F}$	$\mathcal{G}$	$\mathcal{H}$
51.08	26.32	−195.90	−118.31	−3.46	81.74	165.23	228.40	−25.12

time (see Eqs. (61) and (63)). Therefore, these solutions can be interpreted as nonlinear modes, what agrees with theory presented in [36–38].

The approximate amplitude of dispersive modes and the non-dispersive SH mode depends on the $\mathcal{A}$, $\mathcal{B}$ third order and $\mathcal{G}$ fourth order elastic constants. The effect of other nonlinear material constant is negligible. The conclusion follows from the definition of nonlinear stress tensor components – given by Eqs. (9) and (10) – that determine the form of excitation terms in Eq. (32).

The distortion of dispersion curves for the dominant SH modes – generated due to the existence of material nonlinearity – can be observed in the approximate solution. This distortion of dispersion curves is proportional to - $\frac{\mathcal{A}}{4}+\frac{\mathcal{B}}{2}+\mathcal{G}$ i.e., the linear combination of selected nonlinear material constants — and the square of the amplitude of the dominant m_0 SH mode (Eqs. (52) and (59)). In order to illustrate this behaviour, the analytical linear and nonlinear dispersion relations — for selected dominant SH modes with amplitudes equal to 1, 5 and 10 μm are compared in Fig. 3. A 2 mm thick plate with linear and nonlinear material parameters – i.e., the same plate as used in previous numerical simulations (Section 4, Table 1) – are assumed in this analysis. The scale factor of 10 for the component ω_2 in presented dispersion relations – involving amplitudes of dominant modes (Eqs. (52) and (59)) – is applied to distinctly illustrate distortion of dispersion curves. Analogous shifts of the dispersion curves have been previously observed for nonlinear Lamb waves [26].

For all assumed values of amplitudes of the dominant mode, in the low range of frequency and wavenumber, the distortions of the dispersion curves are negligibly small. However, as the frequency, wavenumber and amplitude increase, the differences between the linear and nonlinear curves grow.

For the considered values of linear and nonlinear material parameters, the frequency corresponding to the term ω_2 in Eq. (52) for the dominant SH1 mode is equal to 5.4, 135 and 540 Hz for the wave number $\xi_0 = 2.09$ rad s^{-1} (this wavenumber value results from dispersion relation for the linear SH1 mode for $\omega_0 = 2\,\pi \times 1.3 \times 10^6$ rad s^{-1}) and amplitudes equal to 1, 5 and 10 μm, respectively. For the dominant SH0 mode the frequency corresponding to the term ω_2 in Eq. (59) is equal to 1.9, 47.5 and 190 Hz for wave the number $\xi_0 = 1.41$ rad s^{-1} (this wavenumber value results from dispersion relation for linear SH0 mode for $\omega_0 = 2\pi \times 0.7 \times 10^6$ rad s^{-1}) and amplitudes equal to 1, 5 and 10 μm, respectively.

It is important to note that applicability limits of the presented theory on the distortion of dispersion curves are related to stress values in the material. The state of the system for which dispersion relation is significant could be related to the state of the system for which plastic deformations should appear.

4. Numerical studies of nonlinear shear horizontal waves propagation

In this section, the approximate analytical solution – obtained using the multiple-scale perturbation method for the SH guided wave propagation problem in the Landau–Lifshitz hyperelastic medium – is validated using numerical simulations. Firstly, the derivation of the Local Interaction Simulation Approach (LISA) – implemented for SH wave propagation in arbitrarily nonlinear media – is shortly presented. Then the effect of distributed nonlinearity on shear wave propagation is discussed for a selective excitation of dispersive and non-dispersive SH modes. The modal decomposition and the two-dimensional Fourier transform is used to analyse the simulated wavefields in the wavenumber–frequency domain.

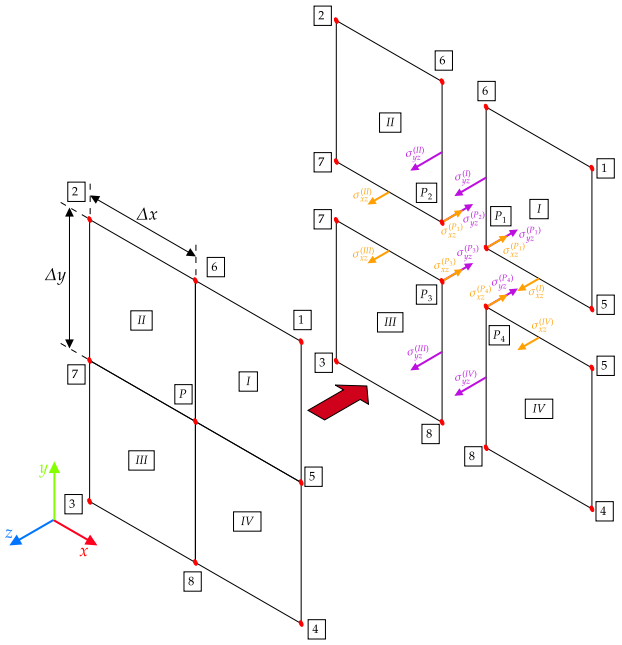

Fig. 4. Discretisation scheme for the LISA approach and stress tensor components used for iteration equation derivation.

4.1. Local interaction simulation approach for shear horizontal wave propagation

The LISA method was firstly proposed in physics for wave propagation modelling in complex media (i.e. media with sharp interfaces and inclusions of different material properties) [48–50]. This modelling technique has been also used extensively for Lamb wave propagation modelling in damage detection studies [51,52]. The work in [13,53] demonstrates the application of LISA for modelling of Lamb waves in hyperelastic medium. The LISA relies on the Finite Difference (FD) formulas in the discrete approximation of the space derivatives in the governing differential equations. The explicit central difference formula is used for time domain discretisation Therefore, the method is well suited for parallel computations, as demonstrated in [54].

For a medium described by two Lagrangian coordinates, the LISA method – implemented for SH wave propagation – discretises the geometrical models of the considered systems into a 2-D grid of rectangular cells. Material properties are assumed to be constant within cells. However, these properties may differ between cells. Thus, the LISA is well suited for wave propagation in complex media that are heterogeneous, anisotropic and nonlinear with sharp material interfaces [49]. The LISA implemented for SH wave propagation in hyper-elastic medium greatly follows the derivation given in [53], thus only a brief description is given here.

Spatial derivatives in the wave propagation Eq. (6) are replaced here by difference formulas in order to obtain the iterative equations for the nonlinear LISA. The iteration equations are derived for nodes located at the intersection (point P) of four adjoining grid cells, as shown in Fig. 4.

For the considered case, this nodal point P belongs to four cells. Each cell is treated as discontinuous and point P is replaced by four points $P^{(i)}$ as shown in Fig. 4. The Navier elastodynamic equation – evaluated at the introduced points $P^{(i)}$ – can be written as

$$\frac{\Delta\sigma_{xz}^{(i)}}{\frac{\Delta x}{2}} + \frac{\Delta\sigma_{yz}^{(i)}}{\frac{\Delta y}{2}} \simeq \rho^{(i)} \frac{\partial^2 w}{\partial t^2}. \tag{64}$$

The finite difference formulas $\Delta\sigma_{xz}^{(i)}$ and $\Delta\sigma_{yz}^{(i)}$ are evaluated for assumed stress component distributions for each cell $I-IV$ presented in Fig. 4. The set of four equations defined by Eq. (64) needs to be completed by enforcing stress continuity between the adjacent cells. This approach leads to the reduction of stress tensor components in Eq. (64). After summing equations for each cell, with imposing stress continuity, the stress-based iteration equation for nodal point P yields

$$\frac{\sigma_{xz}^{(I)} - \sigma_{xz}^{(II)} - \sigma_{xz}^{(III)} + \sigma_{xz}^{(IV)}}{\frac{\Delta x}{2}} + \frac{\sigma_{yz}^{(I)} + \sigma_{yz}^{(II)} - \sigma_{yz}^{(III)} - \sigma_{yz}^{(IV)}}{\frac{\Delta y}{2}} \simeq \sum_i \rho^{(i)} \frac{\partial^2 w}{\partial t^2}. \tag{65}$$

One should note that the presented LISA derivation scheme is based on evaluating the elastodynamic equation and imposing continuity of selected stress tensor components across the cells interfaces. As a result, this procedure can be conducted for the assumed form of the constitutive elastic relation and the geometrical definition of strains.

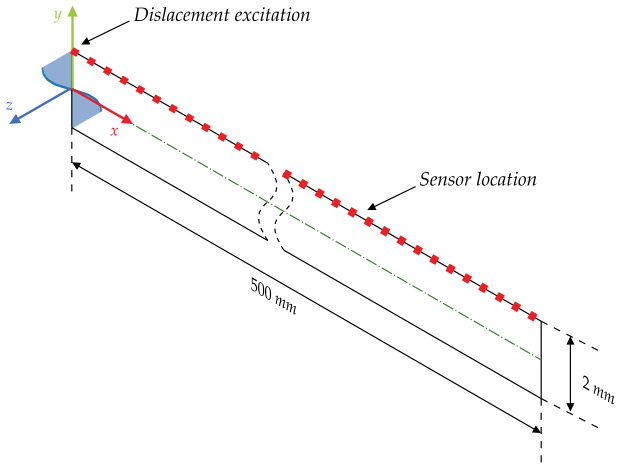

Fig. 5. Two-dimensional 2 mm thick semi-infinite plate model used for the nonlinear wave propagation modelling based on the LISA technique. The SH1 mode is considered in this investigation.

4.2. Numerical model and modes extraction

A 2-D model of a semi-infinite 500 mm plate of 2 mm thickness was simulated. Material properties corresponding to aluminium are assumed to be constant within each of the cells. The adopted linear and nonlinear material parameters used in these simulations are summarised in Table 1. The Landau's TOECs and FOECs values have been calculated on basis of the data presented in [55]. The density $\rho = 2700$ kg/m^3 is assumed.

The dispersion characteristics of linear numerical models – for the given material parameters – are firstly compared with the analytical dispersion curves. The grid dimensions were set to $\Delta x = \Delta y = 0.05$ mm, leading to 40 elements through the thickness of the considered plate. The adopted mesh size in the final numerical model ensures sufficient convergence to the analytical characteristics. The time step for the simulations was set as $\Delta t = 0.01$ μs, to maintain the numerical stability.

The Hanning-windowed 35- and 50-cycle sine burst signals of 0.7 and 1.3 MHz frequency were used to efficiently excite the SH0 and SH1 modes, respectively. The excitation signal was prescribed as a displacement over the thickness of the plate, and assigned to its left-hand side (Fig. 5). The displacement distribution of excitation alongside the y-axis coincided with the selected mode shape. The maximum amplitude of the excitation signal was set as 1 μm.

The wavenumber–frequency characteristic was investigated in order to validate the theory presented in Section 3. The 2-D Fast Fourier Transform was applied to simulated response signals from the top surface of the plate, collected at each time step. The obtained spectra were normalised and expressed in decibels (dB). The maximum value of amplitude spectrum for measurements on the plate surface is treated as a reference level in the calculation of decibel scales for each of the presented results. In addition, the modal decomposition was applied to simulated wavefields in order to verify the analytical results given by Eq. (53). The propagation of nonlinear modeshapes was considered in these simulations. The amplitude of the m-th SH mode is given as

$$A_m(x,t) = \frac{\int_{-h}^{h} Y^{(m)}(y) w(x,y,t) dy}{\int_{-h}^{h} (Y^{(m)}(y))^2 dy}. \tag{66}$$

where $Y^{(m)}(y)$ corresponds to the modeshape of the m-th SH mode of interest, and $w(x,y,t)$ is the displacement field at selected time. The integrals in Eq. (66) are evaluated numerically using the trapezoidal method [56]. This procedure allows one to determine the distributions of the selected SH mode shapes alongside the propagation direction at each simulation step.

4.3. Numerical simulation results for dispersive SH1 and nondispersive SH0 modes

Firstly, the behaviour of the dispersive SH1 mode was examined and compared with the analytical solution given in Section 3. The selected excitation (i.e., a 50-cycle Hanning windowed burst sine signal; central frequency of 1.3 MHz) ensured effective generation of the primary SH1 mode, as shown in Fig. 6.

The theoretical analysis predicts that the interaction of the SH1 mode with the nonlinear material, generates the first harmonic and higher harmonics of odd order (Eq. (61)). This behaviour can be also observed in numerically simulated results, presented in Fig. 6a as dispersion characteristics. Fig. 6b–e compare the contributions of the first four SH modes – i.e. SH0, SH1, SH2 and SH3, respectively – to the complete solution given in Fig. 6a. These analytical contributions were calculated using modal decomposition defined by Eq. (66).

The results show that the characteristics corresponding to the SH0 (Fig. 6b) and SH2 (Fig. 6d) mode shapes do not exhibit higher harmonics, which agrees with the established theory. Numerical errors and the regions of very small amplitudes – corresponding

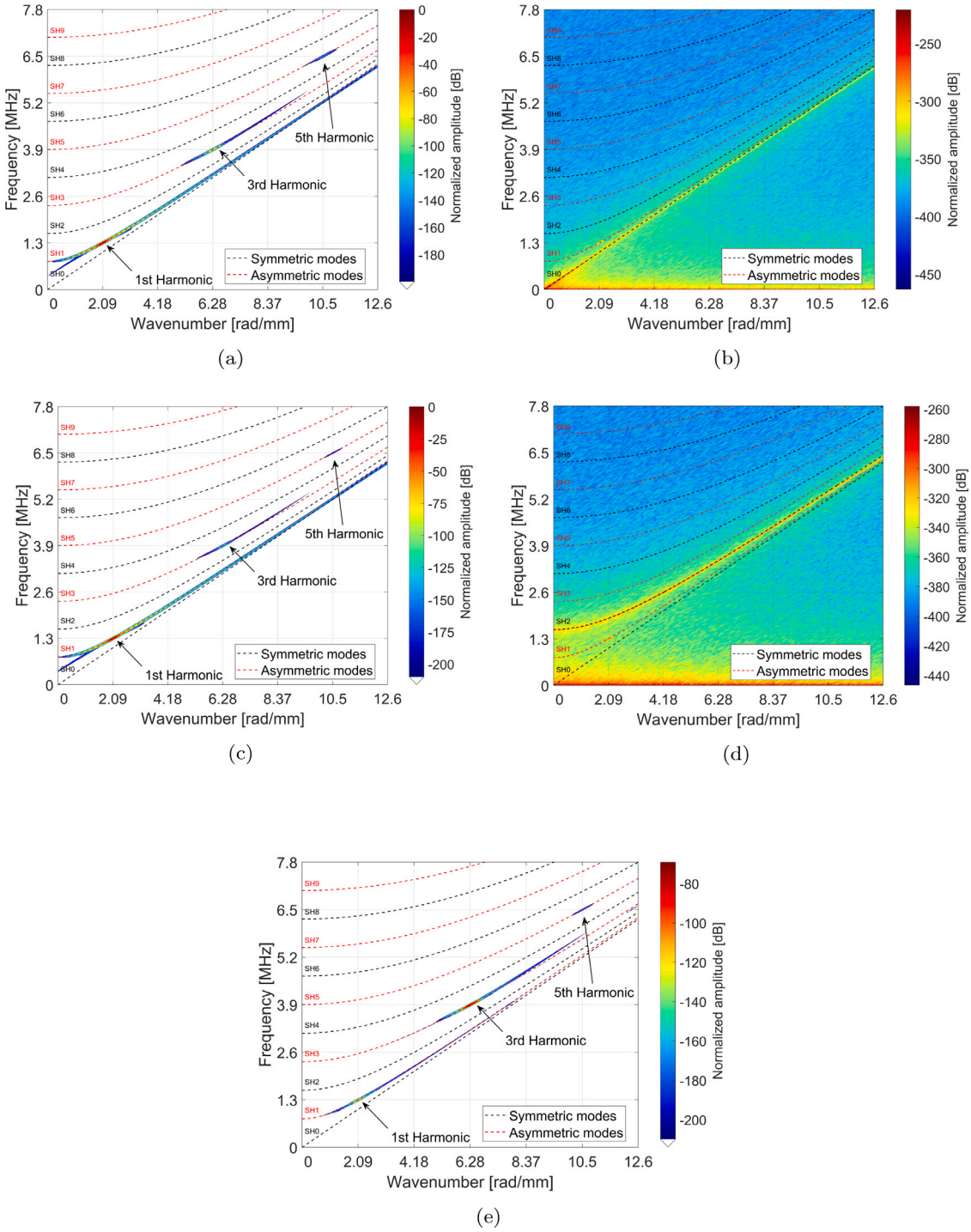

Fig. 6. Frequency–wavenumber representations of the time signals collected for the numerical model with selectively excited SH1 mode (1.3 MHz). The dashed lines correspond to the theoretical dispersion curves. The amplitude characteristics are obtained from: complete solution (a) and the decomposed solutions corresponding to the individual modes shapes: SH0 (b); SH1 (c); SH2 (d) and SH3 (e). Please note that the white background in figures (a), (c) and (e) correspond to numerical amplitudes smaller than −200 dB.

to the dispersion curves for the linear mode shapes – can be only observed. In contrast, the contributions from the SH1 (Fig. 6c) and SH3 (Fig. 6e) mode shapes exhibit odd higher harmonics. Notably, for the SH1 mode shape contribution in Fig. 6c, the first

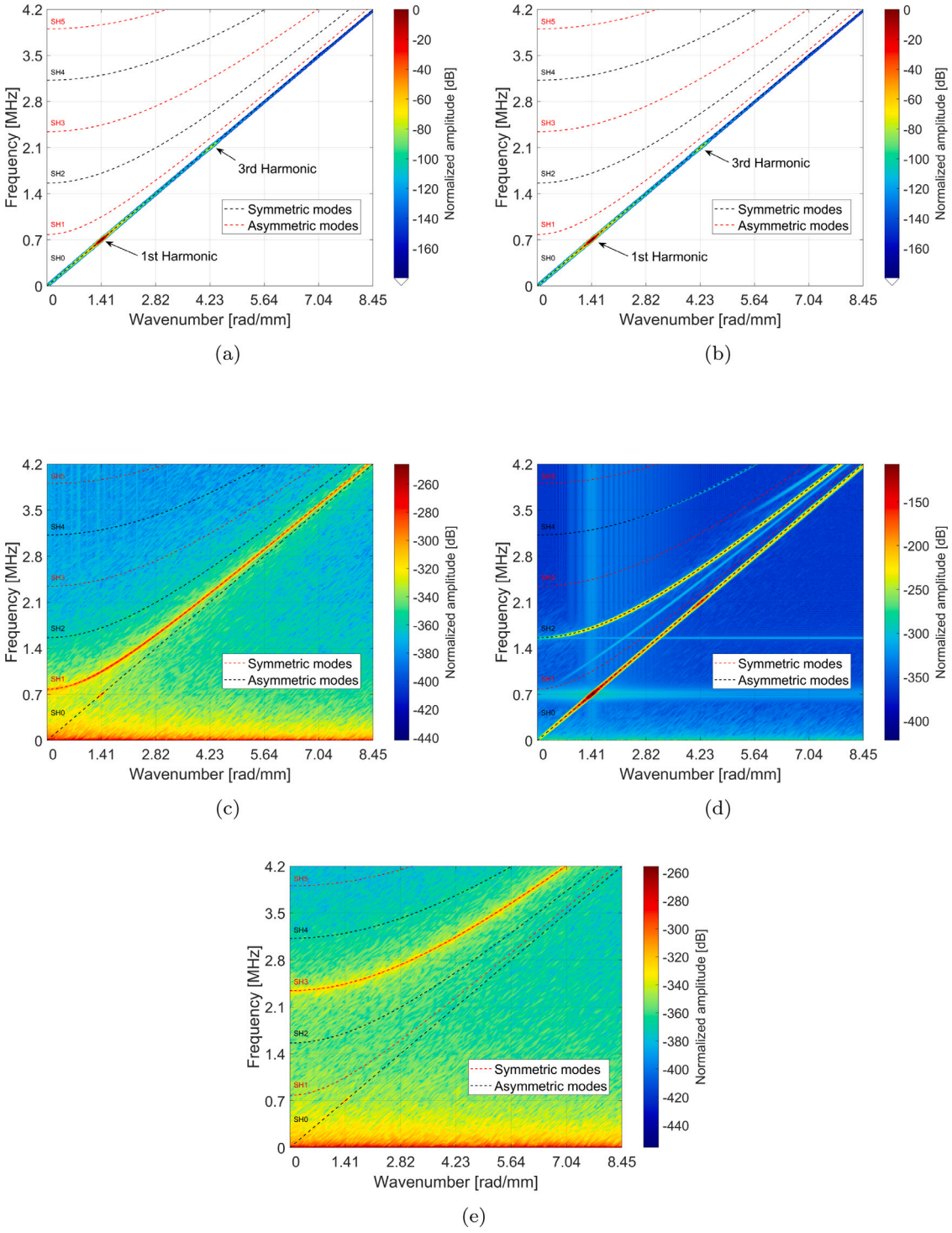

Fig. 7. Frequency–wavenumber representations of the time signals collected for the numerical model with selectively excited SH0 mode (0.7 MHz). The dashed lines correspond to the theoretical dispersion curves. The amplitude characteristics are obtained from: complete solution (a) and the decomposed solutions corresponding to the individual modes shapes: SH0 (b); SH1 (c); SH2 (d) and SH3 (e). Please note that the white background in figures (a), (c) and (e) correspond to numerical amplitudes smaller than −180 dB.

harmonic is a dominant one, while for the SH3 mode shape in Fig. 6e the third harmonic dominates the contribution. This result also agrees well with the analytical solution presented in the previous section.

Secondly, the simulation results corresponding to the SH0 excited mode are presented. This time the excitation burst signal included 35 cycles of sine wave. The excitation was Hanning-windowed. The central frequency was equal to 0.7 MHz.

The theoretical analysis presented in Section 3 indicates that due to the interaction of the SH0 mode with the nonlinear material, the first harmonic and higher odd harmonics should appear in the amplitude spectrum. The theory also predicts that only the SH0 mode shape contribution should be expected in the dispersion characteristics. The simulation results presented in Fig. 7 agree quite well with the developed theory. The dispersion curves for the total response that combines all modes is given in Fig. 7a. The contribution from the SH0, SH1, SH2 and SH3 mode shapes are given in Fig. 7b–e, respectively. Here, the contribution from the SH0 mode shape can be only observed. Numerical errors and small amplitudes corresponding to the dispersion curves for linear mode shapes can be seen in the remaining contributions.

The presented analysis clearly shows that higher harmonics are generated in effect of interaction of the guided SH wave with the material nonlinearity. The level of amplitude change of harmonics – due to wave propagation distance – is very small in our numerical simulations. This is because of the values of nonlinear material parameters and excitation level used in the model. In theory, the amplitude of higher harmonics increases initially and then stabilises with larger distances of wave propagation. This behaviour can be better observed for larger material nonlinearities, as shown in [34]. The displacements field is significantly distorted, and a measure of this distortion can be given as the amplitudes of higher harmonics corresponding to individual mode shapes. Both considered examples i.e., for SH1 and SH0 mode, show agreement with the developed analytical solution.

The shift of the dispersion curves for the excited SH1 and SH0 mods is negligible for the model parameters considered here, as predicted from the analytical solution by Eqs. (52) and (59) (see also Fig. 3).

5. Conclusion

The effect of material nonlinearity – described by the Landau–Lifshitz model – on SH guided wave propagation in plates was investigated theoretically. The major focus was on the effect of nonlinear material parameters, excitation frequency, wavenumber and wave amplitude on nonlinear distortion of the analysed wavefield. Additionally, the analytical definition of dispersion curve shift for the dominant SH mode was calculated. The analytical solution was based on the multiple-scale perturbation method and modal decomposition approach. The approximate analytical solution was validated using the LISA that was implemented specifically for nonlinear shear wave propagation.

The results show that the distortion of the displacement filed can be observed indirectly through the generation of higher harmonics and additional modes together with their higher harmonics. The contributions of individual mode shapes and higher harmonics to the resulting displacement field have been determined using modal decomposition.

The approximate theoretical solution obtained in this paper consists of two parts. The first part represents the wavefield for the dominant SH0 mode in linear material and second part includes other terms that can be interpreted as the nonlinear distortion of the wavefield, which tends to zero as nonlinear parameters vanish. When the movement of particles of considered medium in nonlinear SH wave propagation is analysed, these nonlinear distortions can be interpreted as nonlinear modes. This agrees very well with the vibration theory of nonlinear modes.

The analytical results show that for dispersive modes excited in the plate, the displacement field is distorted alongside the y-axis (i.e., across the thickens of the plate), due to material nonlinearity. As a result, higher harmonics are generated. In contrast, although the nondispersive SH0 mode also generates higher harmonics due to material nonlinearity, the associated displacement wavefield alongside the y-axis (i.e., across the thickness of the plate) is not distorted. The theoretical results show that the third order $\mathcal{A}$, $\mathcal{B}$ and fourth order $\mathcal{C}$ nonlinear elastic constants contribute to the displacement distortion. The remaining nonlinear elastic constants do not affect the analysed SH wavefield.

Numerical simulations confirm all these findings related to higher harmonic generation and distortion of dispersion curves. The numerical approach used – based on the 2-D FFT analysis and modal decomposition – is also capable to estimate the contribution of individual higher modes to the total solution. The distortion of the nonlinear displacement wavefield for dispersive SH guided waves was very small in numerical simulated results. This is mainly due to material parameters and excitation amplitudes used in these investigations.

The theory presented can be used for the analysis of interaction of many SH guided wave modes in plates, which in turn can be utilised for the development of new wave mixing techniques for material/structural damage detection. This could be the subject of future research work in the field.

The results presented in this paper raise the question whether material-related nonlinearities could be separated from nonlinearities produced by the wave interaction with damage (e.g., fatigue cracks). The work presented in this paper is a good starting point to answer this question. Any future work should investigate the interaction of nonlinear SH waves with structural damage. These investigations should be followed by a series of relevant experimental tests.

CRediT authorship contribution statement

M. Osika: Methodology, Software, Validation, Investigation, Writing – original draft, Visualization, Formal analysis. **A. Ziaja-Sujdak:** Software, Investigation, Writing – original draft, Formal analysis. **R. Radecki:** Software, Investigation, Writing – review & editing, Project administration, Formal analysis. **L. Cheng:** Writing – review & editing, Formal analysis. **W.J. Staszewski:** Conceptualization, Writing – review & editing, Supervision, Funding acquisition, Formal analysis.

Data availability

Data will be made available on request.

Acknowledgements

The work presented in this paper was performed within the scope of the research grant UMO-2018/30/Q/ST8/00571 financed by the Polish National Science Centre. This grant is part of the Polish-Chinese collaborative research SHENG initiative nr 51961135302.

References

[1] T. Stepinski, T. Uhl, W. Staszewski, Advanced Structural Damage Detection: From Theory to Engineering Applications, Wiley, 2013.
[2] J. Rose, Ultrasonic Guided Waves in Solid Media, in: Titolo Collana, Cambridge University Press, 2014.
[3] L.K. Zarembo, V.A. Krasil'nikov, Nonlinear phenomena in the propagation of elastic waves in solids, Sov. Phys. Uspekhi 13 (6) (1971) 778–797, http://dx.doi.org/10.1070/pu1971v013n06abeh004281.
[4] I.Y. Solodov, Ultrasonics of non-linear contacts: propagation, reflection and NDE-applications, Ultrasonics 36 (1) (1998) 383–390, http://dx.doi.org/10.1016/S0041-624X(97)00041-3, Ultrasonics International 1997.
[5] C. Lissenden, Y. Liu, J. Rose, Use of non-linear ultrasonic guided waves for early damage detection, Insight - Non-Destr. Test. Cond. Monit. 57 (2015) http://dx.doi.org/10.1784/insi.2015.57.4.206.
[6] C.J. Lissenden, Nonlinear ultrasonic guided waves—Principles for nondestructive evaluation, J. Appl. Phys. 129 (2) (2021) 021101, http://dx.doi.org/10.1063/5.0038340.
[7] M.A. Breazeale, D.O. Thompson, Finite-amplitude ultrasonic waves in aluminum, Appl. Phys. Lett. 3 (5) (1963) 77–78, http://dx.doi.org/10.1063/1.1753876.
[8] M.A. Breazeale, J. Ford, Ultrasonic studies of the nonlinear behavior of solids, J. Appl. Phys. 36 (11) (1965) 3486–3490, http://dx.doi.org/10.1063/1.1703023.
[9] M. Deng, Cumulative second-harmonic generation of Lamb-mode propagation in a solid plate, J. Appl. Phys. 85 (6) (1999) 3051–3058, http://dx.doi.org/10.1063/1.369642.
[10] A. Srivastava, F. Lanza di Scalea, On the existence of antisymmetric or symmetric Lamb waves at nonlinear higher harmonics, J. Sound Vib. 323 (3) (2009) 932–943, http://dx.doi.org/10.1016/j.jsv.2009.01.027.
[11] V.K. Chillara, C. Lissenden, Nonlinear guided waves in plates: A numerical perspective, Ultrasonics 54 (2014) http://dx.doi.org/10.1016/j.ultras.2014.04.009.
[12] W. Ong, W. Chiu, L. Rose, Numerical simulation of cumulative nonlinear symmetric lamb waves in an aluminium plate, Procedia Eng. 188 (2017) 217–224, http://dx.doi.org/10.1016/j.proeng.2017.04.477.
[13] R. Radecki, Z. Su, L. Cheng, P. Packo, W.J. Staszewski, Modelling nonlinearity of guided ultrasonic waves in fatigued materials using a nonlinear local interaction simulation approach and a spring model, Ultrasonics 84 (2018) 272–289, http://dx.doi.org/10.1016/j.ultras.2017.11.008.
[14] Y. Yang, C.-T. Ng, A. Kotousov, Second-order harmonic generation of Lamb wave in prestressed plates, J. Sound Vib. 460 (2019) 114903, http://dx.doi.org/10.1016/j.jsv.2019.114903.
[15] J. Herrmann, J.-Y. Kim, L.J. Jacobs, J. Qu, J.W. Littles, M.F. Savage, Assessment of material damage in a nickel-base superalloy using nonlinear Rayleigh surface waves, J. Appl. Phys. 99 (12) (2006) 124913, http://dx.doi.org/10.1063/1.2204807.
[16] M. Deng, P. Wang, X. Lv, Experimental verification of cumulative growth effect of second harmonics of Lamb wave propagation in an elastic plate, Appl. Phys. Lett. 86 (12) (2005) 124104, http://dx.doi.org/10.1063/1.1891295.
[17] K.H. Matlack, J.-Y. Kim, L.J. Jacobs, J. Qu, Experimental characterization of efficient second harmonic generation of Lamb wave modes in a nonlinear elastic isotropic plate, J. Appl. Phys. 109 (1) (2011) 014905, http://dx.doi.org/10.1063/1.3527959.
[18] A. Nayfeh, Introduction to Perturbation Techniques, in: Wiley Classics Library, Wiley, 2011.
[19] B. Auld, Acoustic Fields and Waves in Solids, in: A Wiley-Interscience Publication, Wiley, 1973.
[20] W. de Lima, M. Hamilton, Finite-amplitude waves in isotropic elastic plates, J. Sound Vib. 265 (4) (2003) 819–839, http://dx.doi.org/10.1016/S0022-460X(02)01260-9.
[21] Y. Liu, V.K. Chillara, C.J. Lissenden, On selection of primary modes for generation of strong internally resonant second harmonics in plate, J. Sound Vib. 332 (19) (2013) 4517–4528, http://dx.doi.org/10.1016/j.jsv.2013.03.021.
[22] Y. Liu, V.K. Chillara, C. Lissenden, J. Rose, Third harmonic shear horizontal and Rayleigh Lamb waves in weakly nonlinear plates, J. Appl. Phys. 114 (2013) 114908, http://dx.doi.org/10.1063/1.4821252.
[23] S. Shengbo, L. Cheng, Mixed third harmonic shear horizontal wave generation: interaction between primary shear horizontal wave and second harmonic Lamb wave, Smart Mater. Struct. 28 (2019) http://dx.doi.org/10.1088/1361-665X/ab1fce.
[24] G. Whitham, Linear dispersive waves, in: Linear and Nonlinear Waves, John Wiley and Sons, Ltd, 1999, pp. 361–402, Ch. 11.
[25] A. Nayfeh, D. Mook, Nonlinear Oscillations, in: Pure and Applied Mathematics: A Wiley Series of Texts, Monographs and Tracts, Wiley, 1979.
[26] P. Packo, T. Uhl, W.J. Staszewski, M.J. Leamy, Amplitude-dependent Lamb wave dispersion in nonlinear plates, J. Acoust. Soc. Am. 140 (2) (2016) 1319–1331, http://dx.doi.org/10.1121/1.4961489.
[27] K. Kanda, T. Sugiura, Internally resonant guided waves arising from quadratic classical nonlinearities with damping, Int. J. Solids Struct. 216 (2021) 250–257, http://dx.doi.org/10.1016/j.ijsolstr.2020.11.033.
[28] D. Mingxi, Cumulative second-harmonic generation accompanying nonlinear shear horizontal mode propagation in a solid plate, J. Appl. Phys. 84 (7) (1998) 3500–3505, http://dx.doi.org/10.1063/1.368525.
[29] W. Li, J. Choi, Y. Cho, Second harmonic generation of shear horizontal guided wave propagation in plate-like structures, Physics Procedia 70 (2015) 451–454, http://dx.doi.org/10.1016/j.phpro.2015.08.283.
[30] R.L. Weaver, Y.-H. Pao, Axisymmetric elastic waves excited by a point source in a plate, J. Appl. Mech. 49 (4) (1982) 821–836, http://dx.doi.org/10.1115/1.3162623.
[31] M. Osika, R. Radecki, A. Ziaja-Sujdak, W.J. Staszewski, Modelling of the shear horizontal waves high-order harmonics generation using local interaction simulation approach, in: P. Rizzo, A. Milazzo (Eds.), European Workshop on Structural Health Monitoring, Springer International Publishing, Cham, 2021, pp. 200–209, http://dx.doi.org/10.1007/978-3-030-64594-6_21.
[32] L.D. Landau, E.M. Lifshitz, Theory of Elasticity, in: Course of Theoretical Physics, Pergamon Press, 1989.
[33] M.F. Hamilton, Y.A. Ilinskii, E.A. Zabolotskaya, Separation of compressibility and shear deformation in the elastic energy density (L), J. Acoust. Soc. Am. 116 (1) (2004) 41–44, http://dx.doi.org/10.1121/1.1736652.

[34] E.A. Zabolotskaya, M.F. Hamilton, Y.A. Ilinskii, G.D. Meegan, Modeling of nonlinear shear waves in soft solids, J. Acoust. Soc. Am. 116 (5) (2004) 2807–2813, http://dx.doi.org/10.1121/1.1802533.
[35] M.S. Wochner, M.F. Hamilton, Y.A. Ilinskii, E.A. Zabolotskaya, Nonlinear torsional wave beams, AIP Conf. Proc. 1022 (1) (2008) 335–338, http://dx.doi.org/10.1063/1.2956224.
[36] A.H. Nayfeh, S.A. Nayfeh, On nonlinear modes of continuous systems, J. Vib. Acoust. 116 (1) (1994) 129–136, http://dx.doi.org/10.1115/1.2930388.
[37] A.H. Nayfeh, On direct methods for constructing nonlinear normal modes of continuous systems, J. Vib. Control 1 (4) (1995) 389–430, http://dx.doi.org/10.1177/107754639500100402.
[38] A.H. Nayfeh, S.A. Nayfeh, Nonlinear normal modes of a continuous system with quadratic nonlinearities, J. Vib. Acoust. 117 (2) (1995) 199–205, http://dx.doi.org/10.1115/1.2873898.
[39] M. Holmes, Introduction to Perturbation Methods, in: Texts in Applied Mathematics, Springer New York, 2012.
[40] J. Kevorkian, J. Cole, Perturbation Methods in Applied Mathematics, in: Applied Mathematical Sciences, Springer New York, 2013.
[41] A. Nayfeh, P. Pai, Linear and Nonlinear Structural Mechanics, John Wiley & Sons, Ltd, 2004, http://dx.doi.org/10.1002/9783527617562.
[42] S. Rao, Solution procedure: Eigenvalue and modal analysis approach, in: Vibration of Continuous Systems, John Wiley and Sons, Ltd, 2006, pp. 151–173, http://dx.doi.org/10.1002/9780470117866.ch6, Ch. 6.
[43] L. Meirovitch, Computational Methods in Structural Dynamics, in: Mechanics: Dynamical Systems, Springer Netherlands, 1980.
[44] L. Meirovitch, Fundamentals of Vibration, Mcgraw-Hill Publ.Comp., 2003.
[45] R.M. Rosenberg, On nonlinear vibrations of systems with many degrees of freedom, Adv. Appl. Mech. 9 (C) (1966) 155–242, http://dx.doi.org/10.1016/S0065-2156(08)70008-5.
[46] A.F. Vakakis, R.H. Rand, Normal modes and global dynamics of a two-degree-of-freedom non-linear system-I. Low energies, Int. J. Non-Linear Mech. 27 (5) (1992) 861–874, http://dx.doi.org/10.1016/0020-7462(92)90040-E, Copyright: Copyright 2014 Elsevier B.V., All rights reserved..
[47] A. Vakakis, R. Rand, Normal modes and global dynamics of a two-degree-of-freedom non-linear system—II. High energies, Int. J. Non-Linear Mech. 27 (5) (1992) 875–888, http://dx.doi.org/10.1016/0020-7462(92)90041-5.
[48] P. Delsanto, T. Whitcombe, H. Chaskelis, R. Mignogna, Connection machine simulation of ultrasonic wave propagation in materials. I: the one-dimensional case, Wave Motion 16 (1) (1992) 65–80, http://dx.doi.org/10.1016/0165-2125(92)90047-6.
[49] P. Delsanto, R. Schechter, H. Chaskelis, R. Mignogna, R. Kline, Connection machine simulation of ultrasonic wave propagation in materials. II: The two-dimensional case, Wave Motion 20 (4) (1994) 295–314, http://dx.doi.org/10.1016/0165-2125(94)90016-7.
[50] P. Delsanto, R. Schechter, R. Mignogna, Connection machine simulation of ultrasonic wave propagation in materials III: The three-dimensional case, Wave Motion 26 (4) (1997) 329–339, http://dx.doi.org/10.1016/S0165-2125(97)00013-9.
[51] B. Lee, W. Staszewski, Modelling of lamb waves for damage detection in metallic structures: Part I. Wave propagation, Smart Mater. Struct. 12 (2003) 804, http://dx.doi.org/10.1088/0964-1726/12/5/018.
[52] B. Lee, W. Staszewski, Modelling of lamb waves for damage detection in metallic structures: Part II. Wave interactions with damage, Smart Mater. Struct. 12 (2003) 815, http://dx.doi.org/10.1088/0964-1726/12/5/019.
[53] P. Packo, R. Radecki, M.J. Leamy, T. Uhl, W.J. Staszewski, Modeling and numerical simulations in nonlinear acoustics used for damage detection, in: T. Kundu (Ed.), Nonlinear Ultrasonic and Vibro-Acoustical Techniques for Nondestructive Evaluation, Springer International Publishing, Cham, 2019, pp. 103–137, http://dx.doi.org/10.1007/978-3-319-94476-0_3.
[54] P. Packo, T. Bielak, A. Spencer, W. Staszewski, T. Uhl, K. Worden, Lamb wave propagation modelling and simulation using parallel processing architecture and graphical cards, Smart Mater. Struct. 21 (2012) http://dx.doi.org/10.1088/0964-1726/21/7/075001.
[55] H. Wang, M. Li, Ab initio calculations of second-, third-, and fourth-order elastic constants for single crystals, Phys. Rev. B 79 (2009) 224102, http://dx.doi.org/10.1103/PhysRevB.79.224102.
[56] G. Dahlquist, A. Bjorck, Numerical Methods in Scientific Computing:: Volume 1, in: Other Titles in Applied Mathematics, Society for Industrial and Applied Mathematics, 2008.